Amplitude equations for the electrohydrodynamic instability in nematic liquid crystals

M. Kaiser and W. Pesch
Physikalisches Institut der Universität Bayreuth, W-8580 Bayreuth, Germany
(Received 22 March 1993)

We study the near-threshold behavior of electrohydrodynamic convection (EHC) in planarly aligned nematic liquid crystals in the (low-frequency) conduction regime. The investigations are based on a rigorous and systematic weakly nonlinear analysis of the standard hydrodynamic equations leading to a reduced description in terms of order-parameter equations. The typical experimental stability regimes in control parameter and wave-number space are identified for normal rolls near threshold. In particular, the decisive role of mean-flow effects in triggering the typical secondary zigzag instability leading to oblique rolls is emphasized. Subsequently, a set of coupled amplitude equations is derived directly from the basic equations that includes the mean-flow effects and higher-order gradient terms important at least in EHC. Simulations of the amplitude equations point to the possible existence of more than one attractor beyond the zigzag destabilization line, which might explain the sometimes conflicting experimental results. The scenario of "weak turbulence" (sometimes called "defect turbulence") is well accounted for by the theory.

PACS number(s): 61.30.−v, 47.20.−k, 47.65.+a

I. INTRODUCTION

The appearance of spatial patterns in fluid systems, driven away from equilibrium, is a common feature in nature [1,2]. The famous canonical example is the Rayleigh-Bénard convection (RBC) in simple fluids, about which many detailed and impressive investigations have been carried out (see, e.g., [3,4]). More recently the electrohydrodynamic instability in a thin layer of a nematic liquid crystal subject to an electric ac field (EHC) has attracted considerable and still growing interest. If the electric field exceeds a certain threshold value, one will observe typical convection-roll patterns roughly as in RBC, and further similarities regarding secondary-bifurcation scenarios are evident (general aspects of EHC are discussed, e.g., in Refs. [5–15]).

On the other hand, there are important differences making EHC interesting in itself. It is presumably the simplest example of an anisotropic pattern forming system, because by means of an appropriate surface treatment a preferred orientation (e.g., planar as in this paper) of the director field $\hat{\mathbf{n}}$, defining the axis of the orientational order in the nematic liquid crystal, can easily be imposed. The electrically driven destabilization mechanism is very effective and rather thin specimens (typical layer thickness from 10 to 100 μm, lateral dimensions of the order of centimeters) with accompanying short relaxation times (below 1 sec) can be used. Because of the large aspect ratio regular patterns of several hundreds or even thousands of rolls are observable and the influence of lateral boundaries is expected to be small, so that the (almost exclusively applied) idealization of a continuous system with infinite extent in two dimensions is well founded. Experimentalists enjoy also the possibility of changing easily several control parameters, such as the frequency of the applied electric field (besides the amplitude) or additional magnetic fields.

For theorists there are further motivations rendering EHC attractive in spite of the challenge presented by the complexity of the system. Already at the onset of the convection instability one has to understand the occurrence of various structures with different space-time symmetries [16,11,14]. Typical are secondary bifurcations near threshold ($\epsilon \gtrsim 0.1$, where ϵ is the usual nondimensional control parameter that is chosen zero at onset). One observes roll patches with alternating directions (zigzag) or sometimes undulations along the roll axis (see, e.g., [17,18]) and transitions to complex spatiotemporal behavior characterized by a continuous generation and annihilation of defects (dislocations) [19–22], which has been described as weak (defect mediated) turbulence [1,23] or fluctuating Williams rolls in the context of EHC [24]. The rich scenario of patterns near threshold makes perturbational calculations promising for EHC, and one can hope to get a better understanding of bifurcation mechanisms observed in RBC normally far above threshold. Anyway, a full Galerkin-type analysis [3] with a subsequent construction of a phase diffusion equation [25] goes to the limit of today's computer facilities for EHC.

The primary goal of this paper is to elucidate the evidently generic features around the secondary zigzag destabilization line, rigorously on the basis of the hydrodynamic equations without flexoelectric effect, as they are used almost exclusively for the description of EHC [11]. We refer always to the standard substance MBBA (*N*-*p*-methoxybenzylidene-*p*-butylaniline), for which most experiments have been made. It is one of the few materials with negative dielectric anisotropy, where all material parameters are known. Like most of the experimental work (or at least the part regarding well-controlled measurements) our investigations refer to the conduction regime for frequencies f below the cutoff frequency f_c [26,11] (several hundred Hz typically), where the slope of the

threshold curve with respect to frequency would diverge. A rough estimate for f_c that works quite well for MBBA is given by $2\pi f_c \tau_0 \geq 2$ [11], where τ_0 denotes the charge relaxation time depending on the conductivity, which can be controlled to some extent by doping.

The perturbation analysis for EHC follows a standard calculational scheme which is more or less well established for continuous extended pattern forming systems near threshold [1,27–29]. The starting point is the hydrodynamic equations, which in the case of EHC couple the electric potential, the velocity, and the director field [5–7,30,31]. Linear perturbation analysis of the quiescent state (spatially uniform director, constant electric field, no velocities in the fluid) yields the threshold voltage and the critical modes. An intuitive physical picture of the basic (Carr-Helfrich-Orsay [32,33,26]) mechanism behind the pattern-forming instability has evolved. Subsequent refinements [34,16,11,14,35,36] led to considerable agreement with experiments in many cases.

To describe the system slightly above threshold in the framework of the weakly nonlinear analysis one can use a wave-packet ansatz (involving a Fourier transformation with respect to the horizontal spatial coordinates) supported by the modes which grow exponentially at threshold or which are only weakly damped (the "active modes" in the notation of [29]). One ends up with order-parameter (OP) equations [27,28] for the expansion coefficients in Fourier space (Fourier amplitudes), by which periodic roll solutions and their stability boundaries can be investigated.

The procedure, which is conceptually clear though tedious because of the complicated structure of the underlying hydrodynamic equations, has been worked out and tested in parallel for EHC and the somewhat simpler situation of RBC [37,38] in nematics. For EHC we always find a forward bifurcation and the typical stability boundaries [20,39], very near threshold involving local compression and dilation of the roll pattern (the generalized Eckhaus process [40,41]), are identified. More importantly, our calculations show very clearly a secondary bifurcation for small but finite $\epsilon \gtrsim 0.05$, where normal-roll patterns lose their stability via a long-wavelength transverse destabilizing mode along the roll axis (called zigzag instability in RBC [3,42]) in agreement with the experimental situation. Moreover, the analysis shows also that the distortion of rolls excites a horizontal "mean-flow" (also called "mean-drift" or "large-scale flow" [1,43,44]) mode with vertical vorticity, which even enforces the distortion.

The reduced dynamical description of EHC by OP equations in Fourier space serves as a convenient starting point for the derivation of the standard amplitude (envelope or Ginzburg-Landau) equations, when transformed to position space by expanding in powers of the Fourier amplitude and its gradients. At leading order in ϵ the resulting amplitude equations [11,41] differ somewhat from the well-known Newell-Whitehead-Segel equations [45,46] for isotropic systems. They were very useful for a universal description of possible patterns near threshold [41,47,11,14] and were also successfully applied to describe the dynamics of defects [48,49,36]. However, the simplest amplitude equation is not sufficient to explain the secondary bifurcation to a zigzag pattern and the weak turbulence mentioned before. This results also from the fact that the amplitude equation in leading order possesses a Lyapunov potential, which has only simple attractors. It will become evident that a set of coupled amplitude equations, which include mean-flow modes, is necessary for an accurate description of the experimental situation in EHC near threshold.

The consideration of large-scale flow effects in nematics originally started with the somewhat artificial (but fashionable) stress- and torque-free boundary conditions [50–52] following the concepts presented in [53]. In that context pattern formation also means spontaneously broken Galilean invariance and the corresponding Goldstone modes have to be treated on the same footing as the modes which trigger the appearance of rolls at threshold. A coupled system of amplitude equations results quite naturally and the coupling of the roll amplitude to the mean flow turns out to be very strong. This leads to an immediate amplification of long-wavelength undulatory fluctuations even at threshold, rendering normal rolls unstable there in contrast to the common experimental situation. The analysis was refined on a purely phenomenological basis and by adjusting the undetermined parameters, some features observed in the experiments could be rediscovered [54–56].

For realistic rigid boundary conditions the derivation of coupled amplitude equations for EHC in nematics starting from a systematic treatment of the basic hydrodynamic equations is conceptually more difficult. The clue is that one ends up with a nonsmooth gradient expansion after simply transforming the OP equation from Fourier to position space. An additional "degree of freedom" has to be introduced that absorbs the singular behavior. We think that our approach, which can be understood as a systematic combination of existing concepts and ideas in the literature [27,29,57,58,53], is a useful contribution also to the general analysis of pattern forming systems.

Since the wave-packet analysis in Fourier space contains as a special case the simple periodic normal-roll patterns and their stability behavior, it is guaranteed by our procedure that long-wavelength stability boundaries calculated from the amplitude equation coincide with those from rigorous calculations. By numerical simulations we were also able to investigate the attractors beyond the stability boundaries. We find that the final state, which is approached after the transients have died out, depends to some extent on the initial conditions. We observe, e.g., undulated and zigzag patterns for the same external parameters, possibly in some relation to metastable states obtained from the amplitude equation near the so-called Lifshitz point [41,36]. That might explain why one has sometimes conflicting experimental results. The tendency towards the spontaneous generation of defects with increasing control parameter ϵ came out very clearly.

The paper is organized in the following manner. In order to ensure the uniformity of the presentation we sketch the well-known underlying equations in Sec. II. In Sec. III the weakly nonlinear analysis is described, and

the typical bifurcation scenarios are presented. In Sec. IV we explain in some detail our method to derive the coupled amplitude equations. In Sec. V a short discussion of possible stability boundaries in the framework of amplitude equations is added. In Sec. VI we discuss the results of our numerical simulations of the coupled amplitude equations. After the conclusion in Sec. VII, the Appendixes contain some technical details and tables of the coefficients of the amplitude equations.

II. THE BASIC EQUATIONS

In this section we provide briefly the basic equations for the description of the electrohydrodynamic instability in nematic liquid crystals [5–7,30,31,59,60,11]. We refer to the usual situation of a planarly oriented nematic layer in the x-y plane sandwiched between conducting plates. The underlying equations couple the electric field $\mathbf{E}$, the director $\hat{\mathbf{n}}$, and the fluid velocity $\mathbf{v}$.

Conservation of charge for a weakly conducting and uniaxial material reads as follows:

$$\begin{aligned} &\mathrm{div}\{\sigma_\perp \mathbf{E}+\sigma_a(\hat{\mathbf{n}}\cdot\mathbf{E})\hat{\mathbf{n}}\}+\frac{d}{dt}\rho_e=0 \ , \\ &\rho_e=\varepsilon_0 \mathrm{div}\{\varepsilon_\perp \mathbf{E}+\varepsilon_a(\hat{\mathbf{n}}\cdot\mathbf{E})\hat{\mathbf{n}}\} \ , \\ &\varepsilon_a=\varepsilon_\parallel-\varepsilon_\perp, \quad \sigma_a=\sigma_\parallel-\sigma_\perp, \quad \frac{d}{dt}=\frac{\partial}{\partial t}+\mathbf{v}\cdot\nabla \ , \end{aligned} \tag{1}$$

ρ_e denotes the charge density, $\varepsilon_\parallel,\varepsilon_\perp$ ($\sigma_\parallel,\sigma_\perp$) are the components of the dielectric (conductivity) tensor parallel and perpendicular to the director, respectively. The electric field can be separated into two parts: The driving ac field in z direction with frequency ω and the induced field, which can be expressed in terms of a potential ϕ:

$$\mathbf{E}=\hat{\mathbf{z}}E_0\cos(\omega t)-\mathrm{grad}\phi \ . \tag{2}$$

With de Gennes's molecular field $\mathbf{h}$ [5] the balance of torques can be written as

$$\mathbf{\Gamma}\equiv\hat{\mathbf{n}}\times\mathbf{h}=\mathbf{0}, \quad \mathbf{h}=\frac{\delta F}{\delta\hat{\mathbf{n}}}-\gamma_1 N-\gamma_2 \mathbf{A}\times\hat{\mathbf{n}} \ . \tag{3}$$

The field $\mathbf{h}$ contains the variational derivative of the orientational free energy F [61]:

$$\begin{aligned} F=&\tfrac{1}{2}k_{11}(\mathrm{div}\hat{\mathbf{n}})^2+\tfrac{1}{2}k_{22}(\hat{\mathbf{n}}\cdot\mathrm{curl}\hat{\mathbf{n}})^2+\tfrac{1}{2}k_{33}(\hat{\mathbf{n}}\times\mathrm{curl}\hat{\mathbf{n}})^2 \\ &-\tfrac{1}{2}\varepsilon_0\varepsilon_a(\hat{\mathbf{n}}\cdot E)^2-\tfrac{1}{2}\mu_0\chi_a(\hat{\mathbf{n}}\cdot\mathbf{H})^2 \end{aligned} \tag{4}$$

describing the elasticity against splay (k_{11}), twist (k_{22}), and bend (k_{33}) deformations of the director field $\hat{\mathbf{n}}$. Besides an electric contribution, F also contains a term that couples to an applied magnetic field $\mathbf{H}$ ($\chi_a=\chi_\parallel-\chi_\perp$, the anisotropy of the magnetic susceptibility tensor χ). The fluid motion leads to viscous torques (with the rotational viscosities γ_1 and γ_2) depending on the rate of change $\mathbf{N}=d\hat{\mathbf{n}}/dt+\frac{1}{2}(\hat{\mathbf{n}}\times\mathrm{curl}\mathbf{v})$ of the director moving with the fluid particles and the hydrodynamic strain tensor $A_{ij}=\frac{1}{2}(\partial v_i/\partial x_j+\partial v_j/\partial x_i)$. Because the three components of Eq. (3) are linearly dependent, we have to single out the projections on a plane locally perpendicular to $\hat{\mathbf{n}}$. An appropriate local coordinate system for our geometry is spanned by the vectors:

$$\hat{\mathbf{n}}, \quad \hat{\mathbf{z}}\times\hat{\mathbf{n}}, \quad \hat{\mathbf{n}}\times(\hat{\mathbf{z}}\times\hat{\mathbf{n}}) \ . \tag{5}$$

The last of our basic equations is the momentum balance (generalized Navier-Stokes equation for an anisotropic system):

$$\rho_m\frac{d\mathbf{v}}{dt}=\mathbf{f}-\mathrm{grad}p+\mathrm{div}\mathbf{T} \ . \tag{6}$$

ρ_m denotes the mass density, $\mathbf{f}=\rho_e\mathbf{E}$ the electric volume force, and p the pressure. We treat the nematic as an incompressible fluid, i.e., $\mathrm{div}\mathbf{v}=0$ with the standard stress tensor

$$\begin{aligned} T_{ij}=&-\sum_k\frac{\partial F}{\partial n_{k,i}}n_{k,j}+\sum_{k,m}\alpha_1 n_k A_{km} n_m n_i n_j+\alpha_2 n_i N_j \\ &+\alpha_3 n_j N_i+\alpha_4 A_{ij}+\sum_k(\alpha_5 n_i n_k A_{kj}+\alpha_6 n_j n_k A_{ki}) \end{aligned} \tag{7}$$

containing the viscosity coefficients α_i. According to the relations

$$\gamma_1=\alpha_3-\alpha_2, \quad \gamma_2=\alpha_3+\alpha_2, \quad \alpha_6-\alpha_5=\alpha_3+\alpha_2 \ , \tag{8}$$

[5,62] the number of independent viscosity coefficients is reduced to five.

A convenient way to satisfy the incompressibility condition is introducing two velocity potentials f and g [63] and expressing $\mathbf{v}$ as

$$\begin{aligned} &\mathbf{v}=\mathrm{curl}\,\mathrm{curl}\hat{\mathbf{z}}f+\mathrm{curl}\hat{\mathbf{z}}g\equiv\underline{\delta}f+\underline{\epsilon}g \ , \\ &\underline{\epsilon}=\left(\frac{\partial}{\partial y},-\frac{\partial}{\partial x},0\right) . \end{aligned} \tag{9}$$

Application of the operators $\underline{\delta}$ and $\underline{\epsilon}$ to the Navier-Stokes equation eliminates the pressure p and two equations for f and g result.

The basic equations have to be supplemented by boundary conditions. We suppose that the velocity vanishes at the confining plates ($z=\pm d/2$, d is the sample thickness) and that the director orientation is held fixed there. This is expressed by the so-called rigid boundary conditions

$$\begin{aligned} &\hat{\mathbf{n}}(\pm d/2)=(1,0,0) \ , \\ &\phi(\pm d/2)=f(\pm d/2)=\partial_z f(\pm d/2)=g(\pm d/2)=0 \ . \end{aligned} \tag{10}$$

In the explicit calculations the equations will be transformed into a dimensionless form by expressing length in terms of d/π, time in terms of $\alpha_0 d^2/k_0\pi^2$, etc. (for details see Appendix A). We introduce, as an analog to the Rayleigh number in thermal convection, the control parameter R, which is proportional to the rms value of the applied voltage $0.5E_0^2/d^2$.

III. WEAKLY NONLINEAR ANALYSIS

For a brief schematic description of the weakly nonlinear analysis it is useful to introduce the deviations

$$\mathbf{V}=(\phi,1-n_x,n_y,n_z,f,g) \tag{11}$$

from the homogeneous solution $n_x=1$, $\phi=n_z=n_y=f=g=0$, which becomes unstable above threshold. The following symbolic notation for the basic equations of Sec. II will be used:

$$\mathcal{L}\mathbf{V}+\mathbf{N}_2(\mathbf{V}|\mathbf{V})+N_3(\mathbf{V}|\mathbf{V}|\mathbf{V})+\cdots = [\mathcal{B}_0+\mathcal{B}_1(\mathbf{V})+\mathcal{B}_2(\mathbf{V}|\mathbf{V})]\frac{\partial \mathbf{V}}{\partial t} . \tag{12}$$

The symbols $\mathcal{L}$ and $\mathcal{B}_i$ represent matrix differential operators of the indicated order in $\mathbf{V}$. The components of the vector operators $\mathbf{N}_2,\mathbf{N}_3,\ldots$ are quadratic, cubic, etc. with respect to the components of $\mathbf{V}$. The explicit form of Eq. (12) is clear from Sec. II, and for our purpose it is not necessary to present the lengthy expressions in detail. All our calculations have been checked with the help of symbolically working systems (MACSYMA, MATHEMATICA).

A. Linear analysis

In order to determine the threshold R_c and the critical wave vector $\mathbf{q}_c$ one has to investigate the linearized problem

$$\mathcal{L}(\partial_x,\partial_y,\partial_z;R)\mathbf{V}=\mathcal{B}_0(\partial_x,\partial_y,\partial_z)\frac{\partial \mathbf{V}}{\partial t} . \tag{13}$$

This has been done in considerable detail during the past years [11,14,35,64,65] and we shall recapitulate very briefly the main results. The operator $\mathcal{L}$ (see Appendix B) contains the external electric ac field, therefore the solution has the general form $\mathbf{V}=e^{\lambda t}\overline{\mathbf{V}}$ (Floquet's theorem), where $\overline{\mathbf{V}}$ has the periodicity of the external field. Equation (13) is then rewritten as

$$\overline{\mathcal{L}}(\partial_x,\partial_y,\partial_z;R)\overline{\mathbf{V}}\equiv\mathcal{L}(\partial_x,\partial_y,\partial_z;R)\overline{\mathbf{V}}-\mathcal{B}_0(\partial_x,\partial_y,\partial_z)\frac{\partial \overline{\mathbf{V}}}{\partial t} =\lambda\mathcal{B}_0(\partial_x,\partial_y,\partial_z)\overline{\mathbf{V}} . \tag{14}$$

As usual one idealizes the convection cell with its large aspect ratio as infinitely extended in the x-y plane, so that the modal solutions have the general form

$$\overline{\mathbf{V}}(x,y,z,t)=\mathbf{V}_0(\mathbf{q},z,t)e^{i\mathbf{q}\cdot\mathbf{x}},\quad \mathbf{q}=(q,p),\quad \mathbf{x}=(x,y) , \tag{15}$$

where the periodic function $\mathbf{V}_0$ can be expanded in a Fourier series

$$\mathbf{V}_0(\mathbf{q},z,t)=\sum_m \mathbf{v}_m(\mathbf{q},z)e^{im\omega t} . \tag{16}$$

The z dependence is treated with a Galerkin method; one expands the velocity potential f in terms of Chandrasekhar functions [66], the other quantities in terms of trigonometric functions, so that the boundary conditions are satisfied [37,38].

If we insert the ansatz (15) and (16) into Eq. (14) the linear equation will be transformed to an infinite-dimensional algebraic eigenvalue problem for the expansion coefficients of $\mathbf{V}(\mathbf{q},z,t)$ (with respect to time and z dependence), which has to be truncated. In this work we are interested in not too thin nematic layers and not too high frequencies (conduction regime [5,11]). The ratio of the director relaxation time and the charge relaxation time (i.e., the parameter Q in Appendix A) is large in that case and it is then possible to take into account only the leading terms with respect to the Fourier expansion in time [11]. The z dependence is well described by only few modes ($\lesssim 5$). In order to perform projections on the space spanned by the eigenmodes of Eq. (14) one also needs the solutions of the adjoint eigenvalue problem, which are analogously found by a double expansion with respect to time and z dependence.

Let $\sigma(\mathbf{q},R)$ be the eigenvalue λ with the maximum real part at given $\mathbf{q}$ and control parameter R. The condition of vanishing real part of σ determines the neutral surface $R_0(\mathbf{q})$. We have never observed a Hopf bifurcation, i.e., the imaginary parts of σ always vanish on the neutral surface. In order to justify our approximation scheme, we have checked carefully that the inclusion of higher Fourier modes in time leaves the bifurcation type unchanged. The minimum of $R_0(\mathbf{q})$ with respect to $\mathbf{q}$ yields the critical wave vector $\mathbf{q}_c=(q_c,p_c)$ and the threshold $R_c=R_0(\mathbf{q}_c)$. Instead of R the dimensionless control parameter $\epsilon=(R-R_c)/R_c$ is often used in the following.

The form of the neutral surface is influenced by the material parameters. For low frequency of the external electrical field and not too small anisotropy of the conductivity tensor (depending also on the other parameters [11]) there are two degenerate minima at $(q_c,\pm p_c)$, i.e., one has oblique rolls at threshold. More frequent is the case of normal rolls, where the neutral surface has a single minimum at $(q_c,0)$, which we exclusively address in this work.

B. Order-parameter equation

The basic idea of the weakly nonlinear analysis [27,28,1,29] (for a recent more detailed presentation see, e.g., [37,38]) is to approximate the solution slightly above threshold by a wave packet of the eigenmodes of Eq. (14) [see also (15) and (16)]:

$$\mathbf{V}\simeq\mathbf{V}_1=\int_{D_+} d\mathbf{q}\, A(\mathbf{q},t)\mathbf{V}_0(\mathbf{q},z,t)e^{i\mathbf{q}\cdot\mathbf{x}}+\text{c.c.} , \tag{17}$$

where $A(\mathbf{q},t)$ reduces the order parameter (amplitude), which vanishes at threshold. The integration domain D_+ is a small area centered at $\mathbf{q}_c$ determined by the condition $\sigma(\mathbf{q},R)\approx 0$, which need not be specified in detail. The amplitude $A(\mathbf{q},t)$ is determined from Eq. (12) by a systematic expansion of $\mathbf{V}$ in terms of the small parameter A in the form $\mathbf{V}=\mathbf{V}_1+\mathbf{V}_2+\mathbf{V}_3+\cdots$. The second-order solution $\mathbf{V}_2$ proportional to A^2 is explicitly calculated as the solution of the corresponding inhomogeneous linear system derived from Eq. (12):

$$\overline{\mathcal{L}}\mathbf{V}_2+\mathbf{N}_2(\mathbf{V}_1|\mathbf{V}_1)=0 . \tag{18}$$

The solution $\mathbf{V}_2$ contains separate contributions with wave vectors near $\pm 2\mathbf{q}_c$ and $\mathbf{q}=0$. The time dependence is again described by a Fourier series and the z dependence by a Galerkin ansatz. Proceeding to third order the equations are closed by projecting $\mathbf{V}_3$ onto the subspace spanned by the linear modes of Eq. (14). The pro-

cedure leads directly to the order-parameter equations in Fourier space

$$a_1(\mathbf{q})\frac{\partial}{\partial t}A(\mathbf{q},t)=a_2(\mathbf{q})A(\mathbf{q},t) + \int_D d\mathbf{q}_1\int_D d\mathbf{q}_2 a_3(\mathbf{q},\mathbf{q}_1,\mathbf{q}_2) \times A(\mathbf{q}_1,t)A(\mathbf{q}_2,t) \times A(\mathbf{q}-\mathbf{q}_1-\mathbf{q}_2,t)\ , \quad (19)$$

where $D=D_+\cup D_-$ with $D_\pm$ being small areas around $\pm\mathbf{q}_c$. The general structure of the equation is immediately clear. The term cubic in A on the right-hand side of (19) has contributions from $\mathbf{N}_3(\mathbf{V}_1,\mathbf{V}_1,\mathbf{V}_1)$ and from $\mathbf{N}_2(\mathbf{V}_1,\mathbf{V}_2)+\mathbf{N}_2(\mathbf{V}_2,\mathbf{V}_1)$ [see (12)]. The coefficients $a_i(\mathbf{q})$ $(i=1,2,3)$ are complicated functions of the material parameters and the external fields, which become accessible only numerically.

To start with we are interested in roll solutions periodic in space characterized by the wave vector $\mathbf{q}_0$, i.e.,

$$A_r(\mathbf{q})=c_r\delta(\mathbf{q}-\mathbf{q}_0)+c_r^*\delta(\mathbf{q}+\mathbf{q}_0)\ . \quad (20)$$

The double integral on the right-hand side of (19) then collapses and the amplitude coefficient c_r is given by

$$|c_r(\mathbf{q}_0)|^2=-\frac{a_2(\mathbf{q}_0)}{a_3(-\mathbf{q}_0,\mathbf{q}_0,\mathbf{q}_0)+a_3(\mathbf{q}_0,-\mathbf{q}_0,\mathbf{q}_0)+a_3(\mathbf{q}_0,\mathbf{q}_0,-\mathbf{q}_0)}\ . \quad (21)$$

Without loss of generality, c_r can be chosen real. It is also obvious that $|c_r|^2$ is proportional to $[R-R_0(\mathbf{q}_0)]/R_0(\mathbf{q}_0)$, the reduced distance from the neutral surface, which serves as our expansion parameter. We found always forward bifurcation with $|c_r(\mathbf{q})|^2\geq 0$ in the interior of the neutral surface.

C. Stability analysis

It is well known that the periodic roll solutions $\mathbf{V}=\mathbf{V}_r$ determined by the ansatz (17) together with Eqs. (20) and (21) are not stable in the whole $\mathbf{q}$ region bounded by the neutral curve $R_0(\mathbf{q})$. The stability analysis of $\mathbf{V}_r$ (see, e.g., [37]) is performed by introducing a linear perturbation $\delta\mathbf{V}_1$ corresponding to a perturbation $\delta A(\mathbf{q},t)$ of the amplitude $\mathbf{A}_r$ [Eq. (20)]:

$$\delta A(\mathbf{q},t)=[c_1(\mathbf{q},\mathbf{s})\delta(\mathbf{q}-\mathbf{q}_0-\mathbf{s})+c_2(\mathbf{q},\mathbf{s})\delta(\mathbf{q}+\mathbf{q}_0-\mathbf{s})]e^{\lambda t}\ . \quad (22)$$

The wave vector $\mathbf{s}$ allows for a modulation of the original pattern. The corresponding second-order perturbation $\delta\mathbf{V}_2$ constructed from Eq. (18) depends linearly on c_1 and c_2 and contains modes with wave vectors $\pm 2\mathbf{q}_0+\mathbf{s}$ and $\mathbf{s}$. At cubic order [see Eq. (12)] the equations are closed by projection onto the linear modes with wave vectors $\mathbf{q}_0\pm\mathbf{s}$. The two resulting linear equations for c_1 and c_2 determine the corresponding growth rate $\sigma_{\text{nonlin}}(\mathbf{q}_0,\mathbf{s})=\text{Re}(\lambda)$. When the maximum of σ_{nonlin} with respect to $\mathbf{s}$ crosses zero from below, a stability boundary of a roll solution with wave vector $\mathbf{q}_0$ (and control parameter R) can be identified. We here consider exclusively long-wavelength modulations with $|\mathbf{s}|\to 0$.

In Fig. 1 a typical stability diagram resulting from our calculations is shown. For $\epsilon\to 0$ one has Eckhaus-like stability boundaries [40] that restrict normal rolls to a region around band center, outside of which the roll pattern becomes unstable against longitudinal modulations parallel to $\mathbf{q}$ [i.e., with $\mathbf{s}=(s_x,0)$]. Note that for $q\geq q_c$ the most dangerous modes are strictly speaking of the skewed-varicose (SV) type [67] with $\mathbf{s}=(s_x,s_y)$, but because of $s_y/s_x\ll 1$ the destabilization is hardly distinguishable from a pure Eckhaus process. More specific and very common for convective instabilities in nematics [19,21,37,38,68,69] is the zigzag (ZZ) instability corresponding to a transverse long-wavelength modulation along the roll axis [i.e., with $\mathbf{s}=(0,s_y)$]. In EHC it does not appear directly at threshold as in isotropic fluids [63], but is shifted slightly above threshold (to a value $\epsilon=\epsilon_{zz}$ in reduced units) and leads to a limitation of the stability regime from above.

The shape of the region where normal rolls are stable is very similar to that known from experiments (see Fig. 1 in [19] or in [21], respectively), where beyond the ZZ line oblique rolls appear. Also the value of ϵ_{zz} at the onset of the ZZ instability fits the experiments quite well. A quantitative comparison is difficult because the precise location of the zigzag instability depends remarkably strong on the material parameters and the frequency. For the strong variation of ϵ_{zz} at band center we give

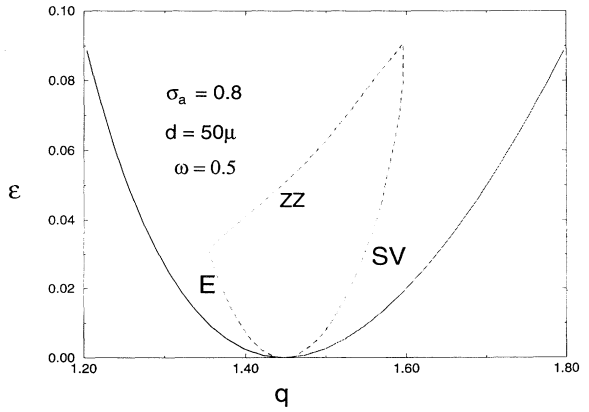

FIG. 1. Stability diagram $[\epsilon=(V^2-V_c^2)/V_c^2]$ vs wave number q for parameters indicated in the figure (see also Appendix A). The solid line denotes the neutral curve, the dashed lines the stability boundaries (E, Eckhaus; SV, skewed varicose; ZZ, zigzag).

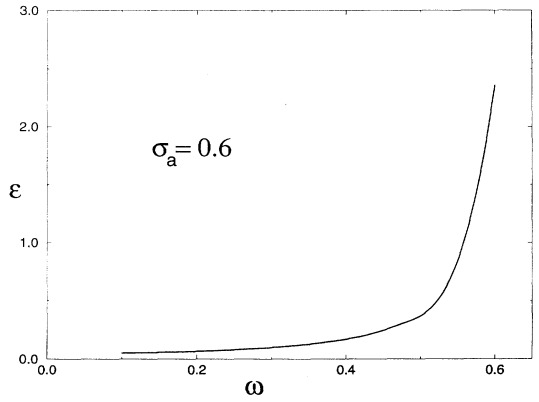

FIG. 2. Onset of the zigzag instability ($\epsilon=\epsilon_{zz}$) at band center ($q=q_c$) as a function of the frequency of the applied voltage in units of the charge relaxation time $\tau_0=\varepsilon_0\varepsilon_\perp/(\sigma_0\sigma_\perp)$ ($\sigma_a=0.6$, otherwise the parameter is the same as in Fig. 1).

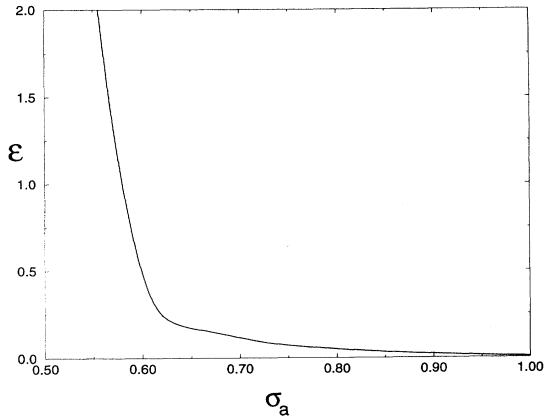

FIG. 3. Onset of the zigzag instability for $q=q_c$ as a function of the conductivity anisotropy σ_a (otherwise the parameter is the same as in Fig. 1).

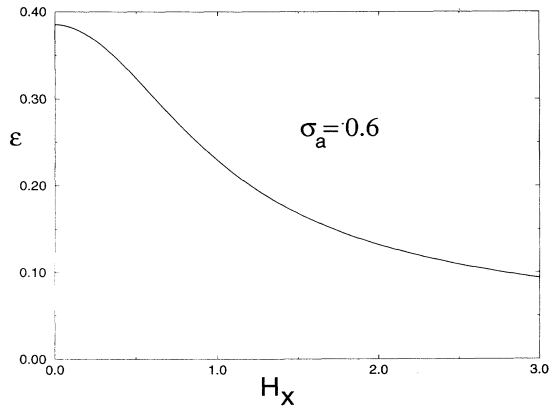

FIG. 4. Onset of the zigzag instability for $q=q_c$ as a function of an applied magnetic field in the x direction ($\sigma_a=0.6$, otherwise the parameter is the same as in Fig. 1).

some examples in Figs. 2 and 3. Especially interesting is the fact that the onset is decreasing if a horizontal (stabilizing) magnetic field is applied (see Fig. 4). That is confirmed in experiments [18,70]. One observes that the distance between the ZZ line and the threshold curve stays nearly constant with increasing magnetic field (see Fig. 6.4 in [12]), corresponding to a decrease of ϵ_{zz}. In the following sections additional results will be given, while we investigate the scenarios beyond the ZZ line in the framework of the amplitude equation formalism.

IV. FROM ORDER PARAMETER TO AMPLITUDE EQUATIONS

In Sec. III we have investigated periodic roll solutions of the order-parameter equations (19) in Fourier space. The description of more complicated patterns, which are observed typically in EHC experiments slightly above threshold, is preferably done in position space. For that purpose one introduces a modulation amplitude $A(\mathbf{x})$ defined as

$$A(\mathbf{x})=\int_{D_+} d\mathbf{q}\, A(\mathbf{q})e^{i(\mathbf{q}-\mathbf{q}_c)\cdot\mathbf{x}} . \tag{23}$$

By the definition of the integration domain D_+ (17) the quantity $\delta q=|\mathbf{q}-\mathbf{q}_c|$ is small in comparison to q_c and correspondingly the amplitude $A(\mathbf{x})$ varies on a scale of the order δq^{-1}. Spatial derivatives of $A(\mathbf{x})$ are given by

$$(-i\partial_x)^m(-i\partial_y)^n A(\mathbf{x}) = \int d\mathbf{q}(q-q_c)^m(p-p_c)^n A(\mathbf{q})e^{i(\mathbf{q}-\mathbf{q}_c)\cdot\mathbf{x}} . \tag{24}$$

The explicit construction of an envelope equation is in principle done by a transcription of the order-parameter equation (19) into position space. The various coefficients a_i have to be expanded into Taylor series around $\mathbf{q}_c$ and translated to spatial derivatives of $A(\mathbf{x})$ [see Eq. (24)]. This works well for the coefficients a_1 and a_2 of the linear part, but does not for a_3 in the cubic part of Eq. (19). While the leading term yields correctly the common $|A|^2A$ contribution of the envelope equation, the direct attempt to produce higher derivatives in the cubic term fails because a_3 has obviously nonanalytic contributions. They are identified as divergencies, if the corresponding derivatives are performed numerically.

By closer inspection and comparison with the simpler case of RBC in isotropic fluids [57,63,43] it is possible to trace back the origin of that nonanalyticity to the second-order terms $\mathbf{V}_2(\mathbf{q})$ with $\mathbf{q}\approx\mathbf{0}$ [see Eq. (18)]. It will become clear in the following that the nonanalyticity is intimately tied to the velocity fields, in particular to a contribution characterized by a nonvanishing spatial average across the convection cell (in z direction). This is the reason why these contributions are called mean-flow terms. They need a special treatment, which will be demonstrated in the following.

A. Calculation of the mean-flow part

The starting point for the calculation of the mean-flow contributions is the inhomogeneous system (18) determin-

ing $\mathbf{V}_2$ with small modulation wave vector $\mathbf{s}$ in the form

$$\mathcal{L}(\mathbf{s})\mathbf{V}_2(\mathbf{s})+\mathcal{J}(\mathbf{s})=\mathbf{0}\ . \tag{25}$$

The inhomogeneity $\mathcal{J}(\mathbf{s})$ derives from the quadratic nonlinearities $\mathbf{N}_2(\mathbf{V}_1,\mathbf{V}_1)$ [see Eq. (18)] by pairwise superposition of contributions from the wave packets $\mathbf{V}_1$ [see (17)] with nearly opposite wave vectors, resulting in slow variations in position space.

As mentioned before the Fourier expansion in time is restricted to the lowest order, which will be sufficient for not too thin cells [11]. Because the long-wavelength modes $\mathbf{V}_2(\mathbf{s})$ are strongly damped solutions of the eigenvalue problem Eq. (14), explicit derivatives with respect to time are neglected in an adiabatic approximation. In the moment both simplifications seem to crucial, when focusing on the derivation of amplitude equations. The approximations can be circumvented in the context of the order-parameter approach (see Sec. III C, or for more details, see [37]) and by comparing the corresponding stability boundaries at most very small quantitative deviations were found.

The complete linear operator $\mathcal{L}$ [Eq. (13)] in position space is shown explicitly in Appendix B. Transformation with respect to the horizontal (x,y) coordinates into Fourier $(\mathbf{s})$ space yields the operator $\mathcal{L}(\mathbf{s})$ [see Eq. (25)]. If only the leading powers in s_x and s_y are kept, Eq. (25) for $\mathbf{V}_2(\mathbf{s})$ with the components (ϕ,n_y,n_z,f,g) reads as follows:

$$-Q\sigma_\perp\partial_z^2\phi=I_\phi=O(1)\ , \tag{26}$$

$$\frac{i}{2}R\varepsilon_a s_x\mathrm{Re}(\phi)-(\tfrac{1}{2}R\varepsilon_a+k_{11}\partial_z^2-H_x^2)n_z +i(k_{22}-k_{11})s_y\partial_z n_y+\frac{i}{2}\alpha_3 s_x\partial_z^2 f+i\alpha_3 s_y\partial_z g =I_{n_z}=O(s_x,s_y^2)\ , \tag{27}$$

$$-i(k_{22}-k_{11})s_y\partial_z n_z+(k_{22}\partial_z^2-H_x^2)n_y=I_{n_y}=O(s_y)\ , \tag{28}$$

$$-\tfrac{1}{2}R(s_x^2+s_y^2)\varepsilon_\perp\partial_z^2\mathrm{Re}(\phi) -\tfrac{1}{2}[\alpha_4(s_x^2+s_y^2)-(\alpha_3+\alpha_6)s_x^2]\partial_z^4 f -\tfrac{1}{2}s_x s_y\partial_z^3(\alpha_3+\alpha_6)g=I_f=O(s_x^2,s_y^2)\ , \tag{29}$$

$$-\tfrac{1}{2}s_x s_y(\alpha_3+\alpha_6)\partial_z^3 f -\tfrac{1}{2}[(\alpha_3+\alpha_6)s_y^2+\alpha_4(s_x^2+s_y^2)]\partial_z^2 g =I_g=O(s_x s_y,s_y^3)\ . \tag{30}$$

The order of magnitude of the components of $\mathcal{J}(\mathbf{s})=(I_\phi,I_{n_y},I_{n_z},I_f,I_g)$ [see Eq. (25)] with respect to s_x,s_y has been indicated. A general presentation of the rather lengthy expressions in $\mathcal{J}(\mathbf{s})$ seems superfluous. One has, for example, a term such as $(\partial_y,-\partial_x)(\mathbf{v}\nabla)\mathbf{v}$ contributing to I_g [originating from the α_4 part of the stress tensor in Eq. (6)], which is well known to trigger the mean flow effects in isotropic fluids [43,44].

It is not difficult to see that the solution vector $\mathbf{V}_2(\mathbf{s})$ of Eqs. (26)–(30) is in general not smooth in the limit $\mathbf{s}\to\mathbf{0}$, except that the quantities I_f,I_g were zero. Therefore we construct $\mathbf{V}_2(\mathbf{s})$ as a linear combination of two contributions. At first we solve Eqs. (26)–(30) for $I_{n_z}=I_{n_y}=0$, from which we get the main nonanalytic contribution. A complementary analytic part of $\mathbf{V}_2$ is obtained when only I_{n_z} and I_{n_y} are kept. It contributes directly to the cubic terms of the amplitude equation and needs no further explanation.

The nonanalytic behavior can be extracted explicitly by direct calculation of ϕ [Eq. (26)], f, and g [Eqs. (29) and (30)] in form of multiple z integrals. The details of that calculation can be found in Appendix C. Both velocity potentials are found to be not smooth if $|\mathbf{s}|=0$ is approached. However, the physical relevant quantities are not f and g, but the resulting velocities, obtained by the application of the operators $\underline{\epsilon}$ and $\underline{\delta}$ [see Eq. (9)]. Consequently, we have to isolate the nonsingular part of the velocities (see again the fairly lengthy calculations in Appendix C). At first one finds that only the horizontal components of the velocity $\mathbf{v}$, namely v_x,v_y, cause problems. The main result is then that the complete nonanalytic part can be deduced from a velocity field with vertical vorticity and a simple z dependence, which can be obtained from the corresponding velocity potential $g_s(\mathbf{s},z)=B(\mathbf{s})(z^2-\pi^2/4)/2$, where $B(\mathbf{s})$ fulfills the equation

$$-\tfrac{1}{2}[(\alpha_3+\alpha_6)s_y^2+\alpha_4(s_x^2+s_y^2)]B =\frac{24}{\pi^3}\int_0^{\pi/2}dz\int_{-\pi/2}^{z}dz'\int_0^{z'}dz''I_g(z'')\ . \tag{31}$$

The singular velocity potential $g_s(\mathbf{s},z)$ can be seen to result from (30) with a modified right-hand side and $f\equiv 0$. Note that it is not sufficient just to take the spatial average of the original inhomogeneity I_g of (30) as proposed tentatively in Ref. [43] for Rayleigh-Bénard convection. The nonanalytical velocities pertaining to Eq. (31) induce via the viscous coupling [Eqs. (27) and (28)] corresponding terms in the director field $\hat{\mathbf{n}}$.

Let us for convenience repeat the main steps and ideas of our procedure: There exists a suitable expression I_g^s [the right-hand side of Eq. (31); the superscript s denotes "singular"], which has to be used to rewrite the right-hand side of Eq. (30) in the form $I_g=I_g^1+I_g^2=(I_g-I_g^s)+I_g^s$. Consequently, the solution of Eqs. (26)–(30) is a superposition of an analytic part resulting from $I_g=I_g^1$ and the nonanalytic one with $I_g=I_g^2$. We have explicitly demonstrated how I_g^s can be constructed in the leading orders in s_x,s_y. The procedure can be continued to arbitrary order in s_x,s_y, if one considers systematically higher order terms in $\mathcal{J}$ and in the linear operator $\mathcal{L}$ (see Appendix B). The calculations are cumbersome in detail, but can be tested at each stage by comparison with the results from Sec. III. In the forthcoming sections it will become clear that the isolation of nonanalytic parts of the OP equations is a necessary first step for the construction of coupled amplitude equations. Also, the question of the uniqueness of the approach and the reasoning by which the expansion with respect to

s_x, s_y has been truncated in the order indicated will be addressed in the following sections.

B. The coupled amplitude equations for EHC

In Sec. IV A we have isolated the nonanalytic part $B(\mathbf{s})$ of the velocity potential g, which is also responsible for certain nonanalyticities in the director field $\hat{\mathbf{n}}$. If one continues the order-parameter expansion up to the third order and keeps the nonanalytic terms separate, one arrives at two coupled integral equations for the amplitudes $A(\mathbf{q})$ and $B(\mathbf{s})$:

$$a_1 \frac{dA(\mathbf{q},t)}{dt} = a_2 A(\mathbf{q}) + \int d\mathbf{q}' \int d\mathbf{q}'' a_3 A(\mathbf{q}') A(\mathbf{q}'') A(\mathbf{q}-\mathbf{q}'-\mathbf{q}'') + \int d\mathbf{s}\, a_4 B(\mathbf{s}) A(\mathbf{q}-\mathbf{s}) , \tag{32}$$

$$b_1 B(\mathbf{s}) = \int d\mathbf{q} b_2 A(\mathbf{q}) A(\mathbf{s}-\mathbf{q}) . \tag{33}$$

The $\mathbf{q}$ integration is confined to the regions $D_{\pm}$ and $|\mathbf{s}|$ is near zero. Equation (33) has been obtained by use of the explicit expression for I_g in Eq. (31). The coefficients a_i and b_i are of course functions of the wave vectors. If one is interested in periodic stationary roll solutions with only one $\mathbf{q}$ mode involved, one recovers back exactly Eq. (21) for the amplitude $A(\mathbf{q})$ because $B(\mathbf{s})$ vanishes rigorously in that case. Even the full Eq. (19) can be recovered if $B(\mathbf{s})$ is inserted in Eq. (32).

The advantage of the present formulation is that by construction all coefficients can now be expanded in powers of $(q-q_c)$, $(p-p_c)$, and s_x, s_y. Equations (32) and (33) are transformed back into position space by means of the definition (23) for the modulation amplitude $A(\mathbf{x})$ and a corresponding one for $B(x,y) \equiv B(\mathbf{x})$ defined by

$$B(\mathbf{x}) = \int d\mathbf{s}\, B(\mathbf{s}) e^{i\mathbf{s}\cdot\mathbf{x}} . \tag{34}$$

In order to get the amplitude equation in the usual form we have rescaled time in terms of a characteristic time T_0 and the amplitude A in terms of $\sqrt{A_{\text{scal}}}$ (see Appendix D). The result is a quite complicated looking system of two coupled amplitude equations:

$$\begin{aligned}
&(1+i\tau_1\partial_x+\tau_2\partial_x^2+\tau_3\partial_y^2)\partial_t A \\
&\quad=\epsilon(1-ie_1\partial_x-e_2\partial_x^2-e_3\partial_y^2+ie_4\partial_x^3+ie_5\partial_x\partial_y^2+e_6\partial_x^4+e_7\partial_x^2\partial_y^2+e_8\partial_y^4)A \\
&\qquad+(r_1\partial_x^2+r_2\partial_y^2+ir_3\partial_x^3+ir_4\partial_x\partial_y^2+r_5\partial_x^4+r_6\partial_x^2\partial_y^2+r_7\partial_y^4)A-|A|^2A-ia_1|A|^2\partial_x A-ia_2A^2\partial_x A^* \\
&\qquad-a_3|A|^2\partial_x^2 A-a_4A^2\partial_x^2A^*-a_5(\partial_x A)^2A^*-a_6|\partial_x A|^2A-a_7|A|^2\partial_y^2A-a_8A^2\partial_y^2A^*-a_9(\partial_y A)^2A^* \\
&\qquad-a_{10}|\partial_y A|^2A+ia_{11}|A|^2\partial_x\partial_y^2A+ia_{12}A^2\partial_x\partial_y^2A^*+ia_{13}(\partial_x\partial_y A)(\partial_y A)A^*+ia_{14}(\partial_x\partial_y A)A\partial_y A^* \\
&\qquad+ia_{15}A(\partial_y A)\partial_x\partial_y A^*+ia_{16}(\partial_y^2 A)(\partial_x A)A^*+ia_{17}(\partial_y^2 A)A\partial_x A^*+ia_{18}A(\partial_x A)\partial_y^2A^*+ia_{19}|\partial_y A|^2\partial_x A \\
&\qquad+ia_{20}(\partial_y A)^2\partial_x A^*-is_1A\partial_y B-s_2(\partial_x A)(\partial_y B)-s_3(\partial_y A)(\partial_x B)-s_4A\partial_x\partial_y B ,
\end{aligned} \tag{35}$$

$$\begin{aligned}
(b_1\partial_x^2+b_2\partial_y^2)B&=q_1\partial_x\partial_y|A|^2+q_2\partial_x(iA\partial_x\partial_y A^*+\text{c.c.})+q_3\partial_y(iA^*\partial_x^2A+\text{c.c.})+q_4\partial_y(iA^*\partial_y^2A+\text{c.c.}) \\
&\quad+q_5(A^*\partial_x\partial_y^3A+\text{c.c.})+q_6(\partial_x A^*\partial_y^3A+\text{c.c.}) .
\end{aligned} \tag{36}$$

Representative numerical values of the coefficients for different experimental parameters can be found in the Appendix D.

The derivation of the amplitude equations (35) and (36) is based on a kind of systematic expansion up to the cubic order in the convection amplitude A, which behaves near threshold as $\sqrt{\epsilon}$. The fact that we have kept more derivative terms than is usually done needs justification. Indeed, if lengths are scaled like $1/\sqrt{\epsilon}$ (in our anisotropic system the same scaling for the x and y coordinates would apply) and time like $1/\epsilon$, one obtains at leading order in ϵ the conventional amplitude equation for anisotropic systems [41]. The quantities $\sqrt{r_1}, \sqrt{r_2}$ are then identified with the parallel and perpendicular coherence lengths $\xi_{\parallel}$ and $\xi_{\perp}$ [11]; the terms $\sim a_i$ in the cubic part of (35) are not included as higher-order contributions in ϵ. Also the mean-flow amplitude B plays no role at that order. The resulting stability boundaries are of the generalized Eckhaus type [41].

The additional higher-order terms are of various nature. First, one has corrections to the time-derivative terms on the left-hand side of Eq. (35) (coefficients τ_i), which are of rather minor importance. Second, one has in the linear operator on the right-hand side of (35) corrections up to fourth order in the derivatives (coefficients e_i and r_i, $i=3,\ldots,7$) corresponding to modifications of the parabolically shaped neutral curve away from band center. Apart from the fact that such corrections can easily be calculated, we found that the description of the pattern beyond the zigzag destabilization (Fig. 1) could be improved to some extent. Furthermore derivative terms in the cubic terms of (35) are included, which will be motivated below in more detail. Of particular importance is the coupling to the mean-flow amplitude B produced by the last four terms in (35), where B is determined from (36). It is obvious that the inversion of the modified Laplacian on the left-hand side of Eq. (36) leads to nonanalytic long-range velocity fields. After all, if one feels certain about the importance of the nonlinear derivative terms, the inclusion of the higher-order terms in the linear operator seems natural for consistency reasons.

In the following section it will be shown that the amplitude equations in the form presented in Eqs. (35) and (36) lead to a satisfactory description of stability regimes of normal rolls with respect to long-wavelength disturbances when one compares with the results of the conventional analysis (see Sec. III). More specifically, we had to keep all higher-order derivatives such as $\partial_x\partial_y^2$ (see the coefficients $a_{11},\ldots,a_{20}$), which are necessary for the calculation of the correct slope of the zigzag destabilization line at band center. Note that their importance cannot be assessed by simple power counting arguments with respect to ϵ. In Sec. VI we will describe simulations of Eqs. (35) and (36) with the conclusion that the resulting pattern are well correlated with the experimental situation.

The general structure of the amplitude equations and of occurring derivative terms is governed by simple symmetry arguments [71]. If the amplitude equation were to be constructed in the oblique-roll regime, even more derivative terms would appear [50]. The coupling between the amplitudes A,B and the structure of the additional B equation can also be compared with the corresponding one in the RBC case [63,43]. One has additional terms in our case because of the anisotropy of the system. Typically higher-order derivatives in the cubic terms are not calculated in the literature, despite their importance for reliable calculations of stability regimes. In any case such terms are of the same order as mean-flow contributions and should appear also for the following consistency reasons. The equation for B contains by construction the singular contributions of the horizontal velocity fields. Their separation from the analytic parts is not unique. One could, e.g., add polynomials in ∂_x,∂_y multiplied by $(b_1\partial_x^2+b_2\partial_y^2)$ applied to $|A^2|$ on the right-hand side of (36), leading to modified coefficients. The corresponding nonsingular contributions for B can be directly calculated and inserted into (35) leading to modified derivative terms in the cubic order, by which the changes in B equation are compensated.

In conclusion we have derived an amplitude equation systematically up to cubic order in A without additional assumptions with respect to length and time scale. The number of derivative terms kept has been judged by comparison with rigorous stability calculations and by consistency requirements. In that respect the coupled amplitude equations serve as a kind of normal form description [72–74] of the stability regimes of EHC near threshold.

V. STABILITY ANALYSIS OF ROLL SOLUTIONS

In this section we shall examine the stability of roll solutions $A_0=Fe^{iQx}$ (the amplitude F and further details of the calculations are presented in Appendix E) of the coupled envelope equations (35) and (36) against long-wavelength perturbations of the form

$$\delta A=e^{iQx}(c_1e^{i(s_xx+s_yy)}+c_2e^{-i(s_xx+s_yy)})e^{\sigma t}\ . \tag{37}$$

The quantity $Q\equiv q-q_c$ denotes the distance from band center. The growth rate σ can easily be determined from a 2×2 eigenvalue problem, where δA is inserted into (35) and (36) by scanning numerically the s_x,s_y for fixed Q and ϵ. Near $Q=0$ one can describe the resulting stability boundaries in more detail. We express the modulation wave vectors s_x and s_y in polar coordinates

$$s_x=S\cos\Theta,\quad s_y=S\sin\Theta \tag{38}$$

and keep only the leading terms in S. Then the reduced growth rate $s(\Theta)\equiv\sigma(\Theta)/S^2$ will be a function of Θ only and can be written as

$$s(\Theta)=\bar a\frac{\sin^4\Theta}{1+v\sin^2\Theta}+\bar b\frac{\sin^2\Theta}{1+v\sin^2\Theta}+\bar c\sin^2\Theta+\bar d\ . \tag{39}$$

The quantities $\bar a$, $\bar b$, $\bar c$, $\bar d$, and v are easily calculated from the coefficients of coupled amplitude equations (35) and (36). It is evident that with the use of Eq. (39) the stability analysis becomes quite transparent and in particular material-parameter studies of EHC are considerably simplified because only the behavior of the five coefficients $\bar a$, $\bar b$, $\bar c$, $\bar d$, and v in Eq. (39) has to be observed.

The various stability boundaries $\epsilon=\epsilon_{\rm stab}(Q)$ are solutions of a quadratic equation in ϵ (see, e.g., Appendix E) obtained from the condition that the global maximum of $s(\Theta)$ becomes for the first time positive at some angle $\Theta=\Theta_0$. One finds first of all a solution corresponding to the Eckhaus instability ($\sin\Theta=0$), which starts quadratically in Q from band center ($\epsilon=0,Q=0$). The corresponding stability boundary $\epsilon_{\rm stab}\equiv\epsilon_{\rm Eck}(Q)$ up to order $\mathcal{O}(Q^3)$ is given by

$$\epsilon_{\rm Eck}(Q)=3r_1Q^2[1-Q(3r_3/r_1-2a_1-3e_1)]\ . \tag{40}$$

In comparison to the neutral curve $[\epsilon_{\rm neutr}(Q)=r_1Q^2+\cdots]$ the curvature of $\epsilon_{\rm Eck}$ at $Q=0$ is larger by the well-known factor 3.

Besides the Eckhaus instability one gets in our case a second solution $\epsilon_{ZZ}(Q)$ (zigzag instability), which confines the stability regime from above (see Fig. 1). It is obtained from Eq. (39), when the coefficients $\bar a,\bar b,\bar c,\bar d$ are expanded up to order $\mathcal{O}(Q)$ (for details see Appendix E). One sees that almost all coefficients of Eqs. (35) and (36) are indeed required for a calculation of the reduced growth rate $s(\Theta)$ and its slope with respect to Q at band center (see Appendix E). The nature of the upper destabilization line can easily be tested with the help of the following criteria.

One would have an Eckhaus-type instability ($\Theta_0=0$, pure modulations along the x direction), if

$$\bar d>0,\quad \bar b+\bar c\le0\ . \tag{41}$$

For the zigzag instability ($\Theta_0=\pi/2$, modulations along the roll axis) one needs

$$\bar a+\bar b+\bar c+\bar d>0,\quad (2+v)(\bar a+v\bar c)+\bar b+\bar c\ge0\ . \tag{42}$$

If the conditions

$$\bar a+v\bar c\le0,\quad (1+v)^2\le\frac{\bar a-v\bar b}{\bar a+v\bar c}\le1 \tag{43}$$

are fulfilled, one would have a skewed-varicose instability ($0\le\Theta_0=\Theta_{\rm SV}\le\pi/2$) with

$$\sin^2\Theta_{SV}=-\frac{1}{v}\left[1-\left[\frac{\bar{a}-v\bar{b}}{\bar{a}+v\bar{c}}\right]^{1/2}\right]. \quad (44)$$

We have tested that the stability boundaries in Fig. 1 agree almost quantitatively with the predictions of the amplitude equations [71]. In particular, the zigzag line and its slope at $Q=0$ is reproduced exactly, as it should be according to our calculational method.

In order to demonstrate in more detail the interplay of the various contributions to the generation of the zigzag instability, e.g., at band center, we give the explicit expression for the value of $\epsilon_{ZZ}(Q=0)$ [see Eq. (E5)] in terms of the coefficients of Eqs. (35) and (36):

$$\epsilon_{ZZ}(Q=0)=\frac{r_2}{e_3+a_7-a_8-2\dfrac{s_1q_4}{b_2}}. \quad (45)$$

First of all, it is significant that the sign of the quantity s_1q_4, which is produced by the mean-flow effects, is negative (note that b_2 is always positive). In RBC this combination is positive with a stabilizing effect, such that with decreasing Prandtl numbers the ZZ instability becomes less important, which for large Prandtl numbers renders rolls with wave vectors $q \lesssim q_c$ unstable (see, e.g., the analytical calculations in [75]). Although we cannot offer a specific mechanism, the situation is apparently generically different in nematics because the same feature is also observed in the RBC for nematics [37,38]. A closer inspection of Eq. (45) shows that in addition to the mean flow the higher derivative terms are of equal importance. From the Tables I and II in Appendix D ($\sigma_a=0.8, \omega\tau_0=0.5, H_x=0$), e.g., we have the following coefficients: $e_3=0.92, a_7=-1.8, a_8=-0.51$, and $2(s_1q_4/b_2)=-1.09$. It is clear that any phenomenological model, where the higher-order derivative terms are typically left out (as in [55,56]), cannot be trusted to produce a correct description of the bifurcation scenarios in EHC.

With the help of the numerically determined coefficients the secondary bifurcation turns out to be always of the ZZ type. Recent experiments [22] indicate another instability, which is attributed to the skewed-varicose type and which for high enough driving frequencies precede the zigzag instability. It is not difficult to model such scenarios by adjusting the coefficients $\bar{a},\bar{b},\bar{c},\bar{d}$ in Eq. (39), as was already recognized in [56], where a set of phenomenological phase diffusion equations leads directly to $s(\Theta)$ in Eq. (39) with $v=0$. However, within the range of material parameters acceptable for MBBA a set of coefficients necessary for a secondary bifurcation of the SV-type could not be obtained.

The amplitude equation can finally be used to describe the situation beyond the secondary bifurcation. As to be expected one has stable oblique-roll solutions of Eqs. (35) and (36) of the form $A_0=Fe^{i(Qx+Py)}$. The amplitude $F(Q,P)$ can easily be calculated and the stability analysis can be performed without difficulty analogous to the normal-roll case ($P=0$) discussed before. Above the zigzag instability, where stable normal-roll solutions do not exist, stable oblique rolls (nonzero P) are still possible. One has a degeneracy between $\pm P$ (zig, zag). In Fig. 5 we compare the stability regime at $Q=0$ (i.e., $q=q_c$) as a function of transverse wave vector P calculated from the coupled envelope equations (35) and (36) and from the "rigorous" order-parameter equation in Sec. III. The inner boundary of the stability regime obtained from the rigorous analysis (diamonds) changes only slightly with $\epsilon(P\approx 0.2,\ 0.08\lesssim\epsilon\lesssim 0.4$ [71]). The corresponding tilt angle of the oblique rolls ($\theta=P/q_c\approx 0.15$) is well correlated with the maximal tilt angle $\theta_m=8°$ found in some experiments [19]. With respect to the amplitude equation there are considerable quantitative deviations for nonzero P. Clearly higher-order derivative terms with respect to y were to be included, which makes it clear that the effort necessary for a quantitative assessment of the secondary bifurcations becomes comparable with a direct solution of the underlying hydrodynamic equations, e.g., by Galerkin methods.

It should be mentioned that the occurrence of stable oblique-roll states beyond the secondary zigzag destabilization is also found in RBC of nematics in the presence of a horizontal magnetic field [37]. In that case even a tertiary short-wavelength instability is predicted connecting the equivalent zig and zag states. A possible final saturated state could be a bimodal structure already observed in RBC experiments [76]. Bimodal structures (also called grid pattern) have also been observed in EHC (see, e.g., [24,10]), and consequently we searched for short-wavelength instabilities in EHC in the framework of OP equations (32) and (33). For commonly used material parameters we could not find such tertiary destabilizations and it cannot be excluded that in EHC they are not contained in the cubic order. That applies also to further long-wavelength destabilizations of oblique rolls [19,21], which could not be detected.

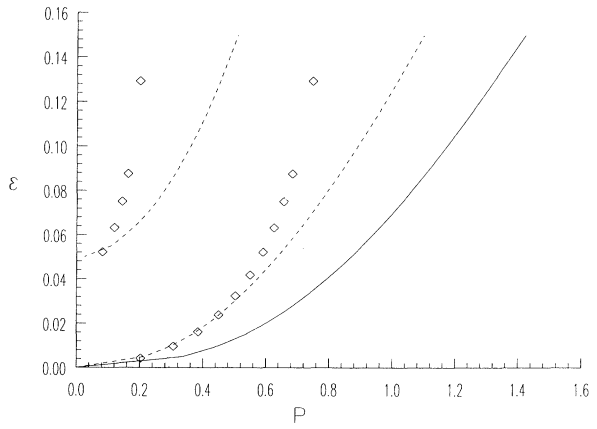

FIG. 5. Stability boundaries regimes for slightly oblique rolls at band center [$\mathbf{q}=(q_c,P)$] calculated from the amplitude equations (35) and (36) (dashed lines) and the more general OP equation (19) (diamonds) in Fourier space (the parameter is the same as in Fig. 1, the solid line denotes the neutral curve).

VI. NUMERICAL SIMULATIONS

We will now describe some representative results of numerical simulations of the coupled amplitude equations (35) and (36). A pseudospectral [fast Fourier transform (FFT)] code in combination with an Adams-Bashforth iteration scheme was used. This method is known to be very stable, though not very precise. We were mainly interested in the possible structures beyond the ZZ destabilization line. For concreteness we have confined ourselves to the parameter set used to calculate the stability diagram displayed in Fig. 1, where the zigzag instability sets in for $\epsilon \approx 0.05$ at band center. It turns out that already simulations in one dimension [disregarding all derivatives with respect to x in (35) and (36)], where one concentrates on the transverse variations responsible for zigzag, provide a rough impression of complex spatiotemporal pattern. Then the amplitude equation explores the stability regimes in the y direction in Fig. 5. In one dimension we have adopted the usual scaling of length, time, and amplitude (see [51]):

$$A' = A/\sqrt{\epsilon}, \quad y' = y\sqrt{\epsilon}/\sqrt{r_2}, \quad t' = t\epsilon \ . \tag{46}$$

The FFT code yields the Fourier coefficients $A_n(t')$ of the amplitude $A(y',t') = \sum_n A_n'(t')\exp(in\Delta p y')$ ($\Delta p = 2\pi/L_y = 0.01$, $-256 \le n \le 256$). If one starts from initial conditions $A_0 \lesssim 1$ (normal rolls) with the other Fourier coefficients random and small ($\lesssim 10^{-3}$) the time development falls into several different cases. For $\epsilon \le 0.05$ the stable normal-role start represents the attractor and the final state is given exactly by $A_0 = 1$, $A_n = 0$ for $n \neq 0$. Beyond the zigzag line, but not too far from it, one has very long transients. Typically a sideband structure is approached as shown in Fig. 6, where the modulus of the A_n is plotted as function of n. One observes a central peak and two large side peaks corresponding to a zig and zag contribution. The position of these peaks corresponds to p values in the stable regime in Fig. 5. The mode distribution is almost steady in Fourier space after the transients have died out and the fine details depend on the initially chosen randomness in the Fourier coefficients. The stable pure zig or zag configurations appear to have only a small basin of attraction. If ϵ is increased further, the central peak vanishes and only the two side peaks survive (see Fig. 7). One has then a situation with pronounced zigs and zags separated by small transition regions. An alternative way to present the results is to display the local wave number $p(y')$, i.e., the derivative of the phase of $A'(y',t')$. In Fig. 8 a snapshot of $p(y)$ is plotted for $\epsilon = 0.1$ as function of y (i.e., in units of the cell thickness d according to $y = y'\sqrt{r_2}/\sqrt{\epsilon} d/\pi$). One finds regular undulations interrupted by rare spikes, which correspond to phase slips at the zeros of $A'(y',t')$. The picture changes dramatically for $\epsilon = 0.2$ as shown in Fig. 9. Now the state contains extended parts with almost constant $p(y') = \pm p$ (pure zig or zag) interrupted by numerous phase slips. From our numerical work we had the impression that there is a kind of phase transition between $\epsilon = 0.1$ and 0.2 where the number of defects increases sharply.

We also performed two-dimensional simulations. The system now has more possibilities to smooth out defects. The usual way to visualize the pattern is to plot the real

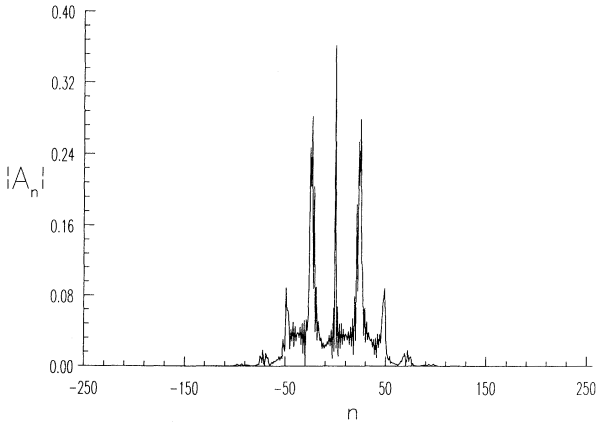

FIG. 6. Typical snapshot of the modulus of the Fourier coefficients A_n (see text) for the 1D simulation at band center for $\epsilon = 0.1$ after the initial transients have decayed (the parameter is the same as in Fig. 1).

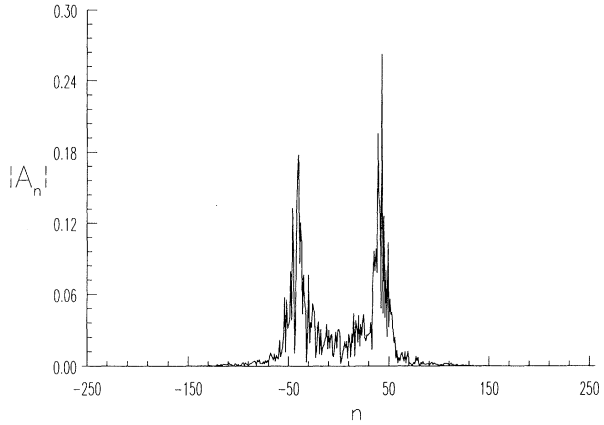

FIG. 7. The 1D Fourier coefficients for $\epsilon = 0.2$ (compare Fig. 6).

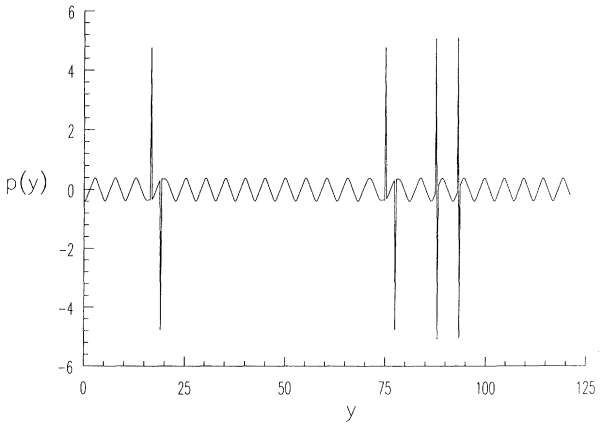

FIG. 8. The local wave number $p(y)$ for $\epsilon = 0.1$. The length is given in units of the cell thickness d (otherwise the parameter is the same as in Fig. 1).

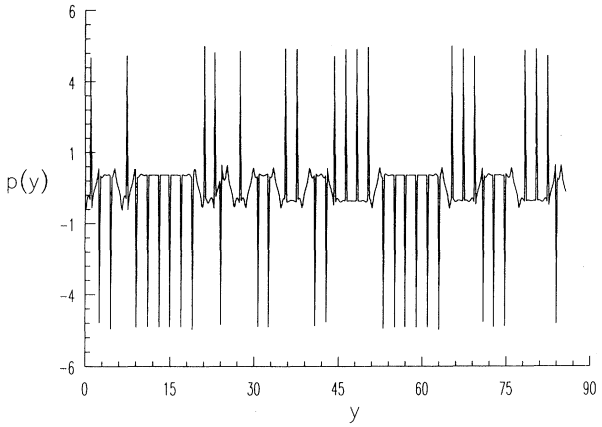

FIG. 9. The local wave number $p(y)$ for $\epsilon=0.2$ (see Fig. 8).

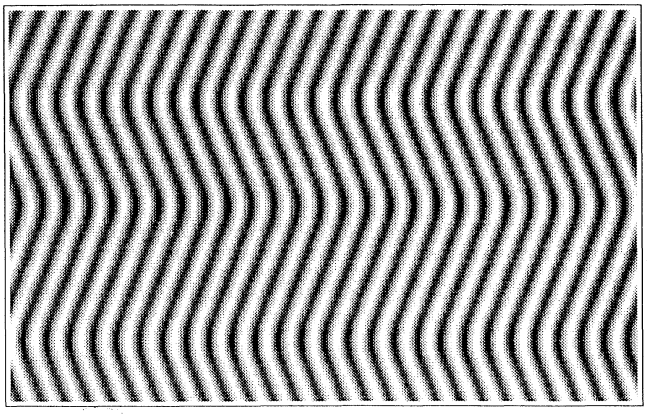

FIG. 11. Snapshot of a stable zigzag pattern (see text) for $\epsilon=0.1$ (the parameter is the same as in Fig. 1).

part of $\exp(iq_c x)A(x,y,t)$. A typical picture for $\epsilon=0.1$ is shown in Fig. 10. The physical length scale can readily be read off from the separation of the rolls, which corresponds to $2d/q_c$ (d is the cell thickness). If one starts from random initial conditions, one observes in most cases an undulated pattern with only a few dislocation defects in close analogy to the one-dimensional case. With respect to their dynamical behavior the defects move slowly on the background of the almost periodic pattern. Alternatively it was also possible to produce a stable zigzag pattern as often observed in experiments, see Fig. 11, if one starts more or less from a sequence of zigs and zags. We were not able to predict systematically, if from the initial conditions a more undulated or a more zigzag pattern would arise. Clearly there is no clear-cut separation between undulations and zigzag in some analogy to the possible pattern at the so-called Lifshitz point [36]. For $\epsilon=0.2$, on the other hand, the pattern always saturated in a state such as that shown in Fig. 12. One observes alternating zigs and zags with more violent dynamics and defects. The basic mechanism behind the typical continuous generation and annihilation of defects ("defect turbulence") can easily be understood. It results from an advection of the roll pattern by the mean flow, which amplifies small undulations. Because the boundary conditions counteract the bending of rolls, the stress is released by straightening the rolls and dislocations are left behind. The situation might correspond to the experimentally observed tertiary bifurcations characterized by fairly large defect densities originating from a destabilization of the undulated or zigzag pattern not far above the ZZ line [19,21]. Obviously such bifurcations are not accessible from a stability analysis of strictly periodic roll solutions as described in Sec. V.

By carefully changing the resolution in space and time we did our best be exclude the possibility that our results are numerical artifacts. In any case we found that the results are very stable running the computer long times without blowup. Obviously only the Fourier modes in the central part of the wave-vector band participate in the long-time behavior (see Figs. 6 and 7). The fact that no short-wavelength modes were produced indicates that the reduced description by the amplitude equations is consistent. Therefore coexistence of several basins of attraction (see Figs. 10 and 11) and the increased average number of defects with increasing ϵ seems quite certain.

In this paper no attempt was made to investigate the

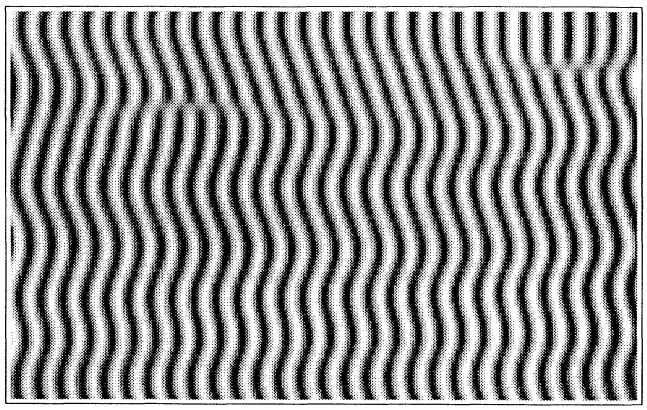

FIG. 10. Snapshot of a 2D simulation pattern (see text) for $\epsilon=0.1$ (the parameters are the same as in Fig. 1) starting from random initial conditions.

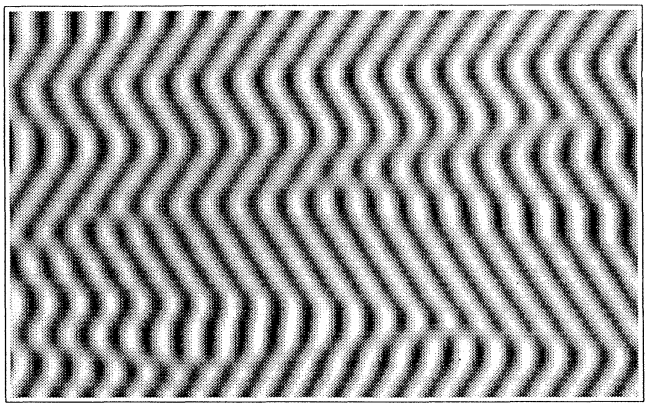

FIG. 12. Snapshot of a 2D simulation pattern for $\epsilon=0.2$ (the parameter is the same as in Fig. 1).

possible scenarios in great detail and to map more exhaustively the solution manifold of the coupled amplitude equations (35) and (36). The main reason is that at first the appropriate mathematical tools for the characterization of complex spatiotemporal behavior have to be developed and tested, work which is just at the beginning [77,78].

VII. CONCLUSION

The main goal of this paper was to present the most general description of EHC near threshold in the framework of a systematic expansion up to cubic order in the convection-roll amplitudes on the basis of the hydrodynamic equations commonly used [11]. At first we arrive at order-parameter equations in Fourier space well suited to investigate possible patterns and their stability near threshold. The secondary zigzag instabilities observed typically in nematics near threshold are born out at least semiquantitatively. The reliability of this approach has also been confirmed recently, when the very rich pattern scenario for RBC in nematics [37] could be reproduced by the much more involved full Galerkin analysis [79].

The central issue of our work concerns the rigorous and consistent derivation of coupled envelope (or amplitude) equations in position space including mean-flow effects, which are necessary for the understanding of the bifurcation scenario in EHC. In order to recover the q dependence of the order parameter and its stability satisfactory in position space, one has in addition to include spatial derivative terms up to fairly high order in the amplitude equation. Because mean-flow effects and higher-order gradient terms are of equal importance determining the secondary stability boundaries [see, e.g., Eq. (55)], a description of EHC by amplitude equations without calculating the coefficients cannot lead to deeper insight.

By numerical simulations we found the occurrence of defect turbulence slightly beyond the secondary zigzag bifurcation. Without reliable mathematical tools we are not sure if the fairly sudden appearance of numerous defects with increasing ϵ can be interpreted as a kind of phase transition, as described in a similar context with traveling waves in EHC [80].

In line with our primary interest we have not presented in this work a detailed parameter study of EHC in nematics contrasted by experiments, but we were satisfied by the identification of the typical experimental scenario for not too high frequencies in the conduction regime. Details of more exhaustive investigations [65] will be presented in a separate paper more addressed to the specialists. There the flexoelectric effect [81,14,82,83] has been included and a large frequency range (including the dielectric regime) is covered. No substantial deviations in the low-frequency range covered by this paper are observed. We never found a secondary bifurcation of the skew-varicose type, as reported in recent experiments [22] for higher frequencies (but still below the cutoff frequency). We are convinced that in this range, where in contrast to theoretical predictions traveling waves are also observed [84,80], the basic equations need improvement [85]. Also a recently proposed new "longitudinal mode" [19] could not be identified. Actually systematic experiments are still missing. Probably much insight would be gained by a controlled variation of the electric conductivity or the dielectric tensor, keeping track of possible accompanying changes of other material parameters (elastic constants, viscosities, etc.), but such measurements are extremely time consuming and special equipment is needed.

We have also applied the same methods to the Rayleigh-Bénard convection in isotropic fluids, where mean-flow effects are of particular importance at low Prandtl numbers. From a technical point of view our method is quite convenient because many ingredients of a Galerkin approach can be incorporated without too much change of existing codes. We obtain again coupled amplitude equations including higher-order gradients. The results of a systematic comparison between order-parameter equations, the amplitude equations, and the full rigorous Galerkin analysis will be presented elsewhere [86].

ACKNOWLEDGMENTS

We wish to thank W. Decker and W. Zimmermann for useful discussions. In particular we are very grateful to L. Kramer for many helpful suggestions and for carefully reading the manuscript.

APPENDIX A: SCALING CONVENTIONS

Throughout this paper we have used the following relations to transform the basic equations into a dimensionless form:

$$
\begin{aligned}
&\text{length} && x = x' \frac{d}{\pi} \\
&\text{time} && t = t' \frac{\alpha_0 d^2}{k_0 \pi^2} \\
&\text{conductivity} && \sigma = \sigma' \sigma_0 \\
&\text{dielectric constant} && \varepsilon = \varepsilon' \varepsilon_0 \\
&\text{electric field} && E = E' E_0 \\
&\text{viscosity coefficients} && \alpha_i = \alpha_i' \alpha_0 \\
&\text{elastic constants} && k_{ii} = k_{ii}' k_0 \\
&\text{magnetic field} && H = H' \frac{\pi}{d} \left[\frac{k_0}{\mu_0 \chi_a} \right]^{1/2} \\
&\text{mass density} && \rho_m = \rho' \frac{\alpha_0^2}{k_0} .
\end{aligned}
\tag{A1}
$$

Viscosity, elasticity constants, and conductivity are typically of the order $\alpha_0 = 10^{-3}$ N s/m^2, $k_0 = 10^{-12}$ N, and $\sigma_0 = 10^{-8}\,(\Omega\,\mathrm{m})^{-1}$, respectively.

After scaling one can identify two characteristic quantities

$$
R = \frac{d^2 \varepsilon_0 E_0^2}{k_0 \pi^2} = \frac{\varepsilon_0 V^2}{k_0 \pi^2} \tag{A2}
$$

and

$$Q=\frac{\alpha_0 d^2\sigma_0}{k_0\pi^2\varepsilon_0} . \tag{A3}$$

R serves as the main control parameter. Q is a measure for the ratio of director and charge relaxation times. The larger Q is, the better an approximation of the temporal behavior with only one Fourier mode it will be. For a much more detailed discussion we refer to [11], where we borrowed also the standard material parameter set (MBBA I in Appendix D of [11]).

APPENDIX B: LINEAR OPERATOR

The linear operator $\mathcal{L}$ (13) (without flexoelectric effect) in dimensionless form reads as follows:

$$-Q(\sigma_\perp\nabla^2+\sigma_a\partial_x^2)\phi=(\varepsilon_\perp\nabla^2+\varepsilon_a\partial_x^2)\partial_t\phi-\varepsilon_a\partial_t(E_0\partial_x n_z) , \tag{B1}$$

$$R\varepsilon_a E_0\partial_x\phi-(R\varepsilon_a E_0^2+k_{33}\partial_x^2+k_{22}\partial_y^2+k_{11}\partial_z^2-H_x^2)n_z+(k_{22}-k_{11})\partial_y\partial_z n_y$$
$$+\tfrac{1}{2}\partial_x[(\alpha_3-\alpha_2)\nabla^2+(\alpha_5-\alpha_6)(\Delta_2-\partial_z^2)]f+\tfrac{1}{2}(\alpha_6-\alpha_5+\alpha_3-\alpha_2)\partial_y\partial_z g=(\alpha_2-\alpha_3)\partial_t n_z , \tag{B2}$$

$$-(k_{22}-k_{11})\partial_y\partial_z n_z+(k_{33}\partial_x^2+k_{11}\partial_y^2+k_{22}\partial_z^2-H_x^2)n_y+(\alpha_5-\alpha_6)\partial_x\partial_y\partial_z f$$
$$+\tfrac{1}{2}[(\alpha_2-\alpha_3)\Delta_2+(\alpha_6-\alpha_5)(\partial_x^2-\partial_y^2)]g=-(\alpha_2-\alpha_3)\partial_t n_y , \tag{B3}$$

$$RE_0\Delta_2(\varepsilon_\perp\nabla^2+\varepsilon_a\partial_x^2)\phi-R\varepsilon_a E_0^2\partial_x\Delta_2 n_z+[\alpha_1\partial_x^4\partial_z^2+\tfrac{1}{2}(\alpha_5-\alpha_2)\partial_x^2\nabla^2\Delta_2+\tfrac{1}{2}\alpha_4\nabla^4\Delta_2+\tfrac{1}{2}(\alpha_3+\alpha_6)\partial_x^2\partial_z^2\nabla^2]f$$
$$+\tfrac{1}{2}\partial_x\partial_y\partial_z[2\alpha_1\partial_x^2+(\alpha_3+\alpha_6)\nabla^2]g=(\alpha_2\Delta_2-\alpha_3\partial_z^2)\partial_x\partial_t n_z-(\alpha_2+\alpha_3)\partial_x\partial_y\partial_z\partial_t n_y+\rho_m\nabla^2\Delta_2\partial_t f , \tag{B4}$$

$$\tfrac{1}{2}\partial_x\partial_y\partial_z[2\alpha_1\partial_x^2+(\alpha_3+\alpha_6)\nabla^2]f+[\alpha_1\partial_x^2\partial_y^2+\tfrac{1}{2}(\alpha_5-\alpha_2)\partial_x^2\Delta_2+\tfrac{1}{2}(\alpha_3+\alpha_6)\partial_y^2\nabla^2+\tfrac{1}{2}\alpha_4\nabla^2\Delta_2]g$$
$$=-\alpha_3\partial_y\partial_z\partial_t n_z+(\alpha_2\partial_x^2-\alpha_3\partial_y^2)\partial_t n_y+\rho_m\Delta_2\partial_t g . \tag{B5}$$

$E_0=\cos(\omega t)$ denotes the applied voltage and $\Delta_2=\partial_x^2+\partial_y^2$ is the horizontal Laplacian. The normalization of the linear eigenvector has been fixed by choosing the leading expansion coefficient of the velocity potential f (with respect to time and z dependence) equal to one. Multiplication with the amplitude A [determined from the order-parameter equation (19) or from the coupled amplitude equation (35) and (36)] yields detailed information about the physical quantities above threshold.

APPENDIX C: CALCULATION OF THE MEAN-FLOW PART

In this appendix we describe in some detail how the nonanalytic behavior is extracted from Eqs. (26)–(30) in Sec. IV (see also [71]). In a first step all variables except f are eliminated as follows. Equation (26) is solved first by integration with respect to z and the resulting electric potential ϕ is inserted into the other equations. Furthermore we use a more explicit form for the inhomogeneities I_f, I_g, which have been constructed from the inhomogeneities of the momentum equation (6) $I_{v_x}, I_{v_y}, I_{v_z}$ with the help of the operators $\underline{\delta}, \underline{\epsilon}$ [see Eq. (9)]. In Fourier space we have [the $(\mathbf{s},z)$ dependence of the I_{v_i} is suppressed in the following]

$$\begin{aligned} I_g &= is_y I_{v_x}-is_x I_{v_y} , \\ I_f &= is_x\partial_z I_{v_x}+is_y\partial_z I_{v_y}-(s_x^2+s_y^2)I_{v_z} , \end{aligned} \tag{C1}$$

and Eq. (29) after insertion of (30)

$$-[as_x^2+(a+b)s_y^2]\partial_z^2 g=is_y I_{v_x}-is_x I_{v_y}+bs_x s_y\partial_z^3 f \tag{C2}$$

appears in the form

$$a(a+b)(s_x^2+s_y^2)\partial_z^4 f=ias_x\partial_z A_1+i(a+b)s_y\partial_z A_2$$
$$+[as_x^2+(a+b)s_y^2]A_3 . \tag{C3}$$

For convenience, we use the abbreviations

$$a=\frac{\alpha_4}{2},\quad b=\frac{\alpha_3+\alpha_6}{2} , \tag{C4}$$

and in a more compact notation A_1 and A_2 instead of I_{v_x} and I_{v_y}, respectively, A_3 is a combination of I_{v_z}, and the contribution of the electric potential ϕ [see Eq. (29)],

$$A_3=I_{v_z}+\tfrac{1}{2}R(s_x^2+s_y^2)\varepsilon_\perp\partial_z^2\mathrm{Re}(\phi) . \tag{C5}$$

For the moment we write Eq. (C3) in a condensed form:

$$\partial_z^4 f=F(z) , \tag{C6}$$

where F is an abbreviation for the right-hand side of Eq. (C3) divided by $a(a+b)(s_x^2+s_y^2)$. The solution of (C6), which satisfies the boundary conditions (10), is given by

$$f(z)=\int_0^z dz'\int_{-\pi/2}^{z'}dz''\int_0^{z''}dz'''\int_{-\pi/2}^{z'''}dz''''F(z'''')$$
$$+\frac{4J}{\pi^3}z\left[z^2-\frac{3\pi^2}{4}\right] \tag{C7}$$

with the integration constant

$$J=\int_0^{\pi/2}dz'\int_{-\pi/2}^{z'}dz''\int_0^{z''}dz'''\int_{-\pi/2}^{z'''}dz''''F(z'''') \ . \quad \text{(C8)}$$

The result for f is inserted into Eq. (C2), which can be written as

$$\partial_z^2 g=G(z) \ . \quad \text{(C9)}$$

The quantity $G(z)$ is the right-hand side of Eq. (C2) divided by $[as_x^2+(a+b)s_y^2]$. Equation (C9) is solved (observing the boundary conditions) by

$$g(z)=\int_{-\pi/2}^{z}dz'\int_0^{z'}dz''G(z'') \ . \quad \text{(C10)}$$

It is obvious that $g(z)$ is nonanalytic because of the quadratic form in s_x,s_y on the left-hand side of Eq. (C2) and that applies analogously to f by inspection of Eq. (C3). The nonanalytic part (or, equivalently, the mean-flow part) of the horizontal velocity v_x is obtained by the application of the operators $\underline{\epsilon}$ and $\underline{\delta}$ [see Eq. (9)] on the velocity potentials f and g and disregarding finally contributions which can be written in the form of a power series in s_x and s_y. A corresponding calculation for v_y leads to analogous conclusions. The x component of the velocity reads

$$\begin{aligned} v_x &= is_x\partial_z f+is_y g \\ &= is_x\int_{-\pi/2}^{z}dz'\int_0^{z'}dz''\int_{-\pi/2}^{z''}dz'''F(z''') \\ &\quad +is_x\frac{12J}{\pi^3}\left[z^2-\frac{\pi^2}{4}\right]+is_y\int_{-\pi/2}^{z}dz'\int_0^{z'}dz''G(z'') \ . \end{aligned} \quad \text{(C11)}$$

After insertion of F, G, and J and some rearrangement one gets

$$\begin{aligned} v_x &= \frac{12as_x^2}{\pi^3(a+b)[as_x^2+(a+b)s_y^2]}\left[z^2-\frac{\pi^2}{4}\right]\int_0^{\pi/2}dz\int_{-\pi/2}^{z}dz'\int_0^{z'}dz''\int_{-\pi/2}^{z''}d\xi\,A_1(\xi) \\ &\quad +\frac{as_x^2}{(a+b)[as_x^2+(a+b)s_y^2]}\int_{-\pi/2}^{z}dz'\int_0^{z'}dz''\int_{-\pi/2}^{z''}d\xi\,A_1(\xi)+\frac{s_y^2}{as_x^2+(a+b)s_y^2}\int_{-\pi/2}^{z}dz'\int_0^{z'}d\xi\,A_1(\xi) \\ &\quad +\frac{12s_xs_y}{\pi^3[as_x^2+(a+b)s_y^2]}\left[z^2-\frac{\pi^2}{4}\right]\int_0^{\pi/2}dz\int_{-\pi/2}^{z}dz'\int_0^{z'}dz''\int_{-\pi/2}^{z''}d\xi\,A_2(\xi) \\ &\quad +\frac{s_xs_y}{[as_x^2+(a+b)s_y^2]}\int_{-\pi/2}^{z}dz'\int_0^{z'}dz''\int_{-\pi/2}^{z''}d\xi\,A_2(\xi)-\frac{s_xs_y}{as_x^2+(a+b)s_y^2}\int_{-\pi/2}^{z}dz'\int_0^{z'}d\xi\,A_2(\xi) \\ &\quad -\frac{12is_x}{\pi^3(a+b)}\left[z^2-\frac{\pi^2}{4}\right]\int_0^{\pi/2}dz\int_{-\pi/2}^{z}dz'\int_0^{z'}dz''\int_{-\pi/2}^{z''}d\xi\,A_3(\xi) \\ &\quad -\frac{is_x}{(a+b)}\int_{-\pi/2}^{z}dz'\int_0^{z'}dz''\int_{-\pi/2}^{z''}d\xi\,A_3(\xi) \ . \end{aligned} \quad \text{(C12)}$$

The z integrals can be simplified after splitting the A_i $(i=1,2)$ in the layer average A_i' and the rest A_i'' resulting in

$$\begin{aligned} v_x &= -\frac{is_x}{a+b}\left[1+\left[z^2-\frac{\pi^2}{4}\right]\frac{12}{\pi^3}\int_0^{\pi/2}dz\right]\int_{-\pi/2}^{z}dz'\int_0^{z'}dz''\int_{-\pi/2}^{z''}d\xi\,A_3(\xi) \\ &\quad +\frac{1}{a+b}\left[1+\left[z^2-\frac{\pi^2}{4}\right]\frac{12}{\pi^3}\int_0^{\pi/2}dz\right]\int_{-\pi/2}^{z}dz'\int_0^{z'}dz''A_1''(z'') \\ &\quad -\frac{s_y^2}{as_x^2+(a+b)s_y^2}\left[z^2-\frac{\pi^2}{4}\right]\frac{12}{\pi^3}\int_0^{\pi/2}dz\int_{-\pi/2}^{z}dz'\int_0^{z'}dz''A_1''(z'') \\ &\quad +\frac{s_xs_y}{as_x^2+(a+b)s_y^2}\left[z^2-\frac{\pi^2}{4}\right]\frac{12}{\pi^3}\int_0^{\pi/2}dz\int_{-\pi/2}^{z}dz'\int_0^{z'}dz''A_2''(z'') \\ &\quad +\frac{1}{2}\left[z^2-\frac{\pi^2}{4}\right]\left[\frac{s_y^2}{as_x^2+(a+b)s_y^2}A_1'-\frac{s_xs_y}{as_x^2-(a+b)s_y^2}A_2'\right] \ . \end{aligned} \quad \text{(C13)}$$

The first two terms contain contributions to v_x regular for $\mathbf{s}\to\mathbf{0}$, while the remaining ones correspond to the mean-flow part, characterized by a nonunique limit for vanishing $\mathbf{s}$. Note in addition that the third and fourth summands stem from the integration constant J in the f equation and cannot be obtained by simply averaging the original inhomogeneity in the g equation as sometimes indicated [29]. Using the identity

$$\int_0^{\pi/2}dz\int_{-\pi/2}^{z}dz'\int_0^{z'}dz''=-\frac{\pi^3}{24} \ , \quad \text{(C14)}$$

the singular part of (C13) can be written in a more compact form:

$$v_x^s=\frac{-12}{\pi^3}\left[z^2-\frac{\pi^2}{4}\right]\frac{is_y}{as_x^2-(a+b)s_y^2}\times\int_0^{\pi/2}dz\int_{-\pi/2}^{z}dz'\int_0^{z'}dz''I_g(z'')\ . \tag{C15}$$

The calculation for v_y would be similar: One gets the same expression, where only the prefactor $-is_y$ has to be substituted by is_x in front of integral in (C15). We conclude that the nonanalytic components of the horizontal velocity field can be deduced from the nonanalytic velocity potential $g_s(\mathbf{s},z)=\frac{1}{2}B(\mathbf{s})(z^2-\pi^2/4)$ with B given in Sec. IV A [Eq. (31)], transformed into position space, in accordance with

$$v_x^s=\partial_y g_s,\quad v_y^s=-\partial_x g_s\ . \tag{C16}$$

APPENDIX D: COEFFICIENTS OF THE AMPLITUDE EQUATIONS

In this appendix we give some examples for coefficients of the coupled amplitude equations (35) and (36) for different values of the anisotropy σ_a of the conductivity, the frequency ω, and magnetic fields H_x. Otherwise the calculations rely on the standard material parameters for MBBA (MBBA I in Appendix D of [11]). The dimensionless units of Appendix A have been used throughout with exception of ω, which is measured in the conventional physical units (time scale determined by the charge relaxation time $\tau_0=\varepsilon_0\varepsilon_\perp/\sigma_0\sigma_\perp$). Note that the coefficients b_1 and b_2 (36) are given by $b_1=0.5\alpha_4$ and $b_2=0.5(\alpha_4+\alpha_3+\alpha_6)$ with the numerical values $b_1=41.3$ and $b_2=23.95$ for our standard parameter set.

Table I contains linear and nonlinear coefficients for zero magnetic field $H_x=0$; the corresponding ones for $H_x=1$ can be found in Table II. The numerical values have been included more for completeness, and by inspection no significant changes in the dependence on the material parameters can be observed. A complicated interplay of the coefficients determines the stability boundaries as shown, e.g., in Figs. 1–5 according to Eqs. (39) and (45). Additional coefficient sets for other material parameters are available upon request from the authors.

APPENDIX E: STABILITY ANALYSIS OF THE AMPLITUDE EQUATIONS

Using Eq. (35) a roll solution of the form $A_0=Fe^{iQx}$ can easily be obtained with the amplitude F:

$$F^2=\frac{\epsilon(1+e_1Q+e_2Q^2+e_4Q^3+e_6Q^4)-r_1Q^2+r_3Q^3+r_5Q^4}{1-(a_1-a_2)Q-(a_3+a_4+a_5-a_6)Q^2}\ . \tag{E1}$$

The growth rate σ is calculated using the ansatz (37) for the perturbation δA. Because we are interested in long-wavelength instabilities, it is sufficient to keep only the terms quadratic with respect to s_x and s_y in σ. After some calculation one gets

$$\begin{aligned}\sigma=&\frac{1}{T}(L^{xx}+N_1^{xx}-N_2^{xx})s_x^2+\frac{1}{T}(L^{yy}+N_1^{yy}-N_2^{yy})s_y^2\\&+2\frac{B_1}{T}\frac{(s_xs_y)^2}{b_1s_x^2+b_2s_y^2}+2\frac{B_2}{T}\frac{s_y^4}{b_1s_x^2+b_2s_y^2}\\&-\frac{(L^x+N_1^x+N_2^x)(L^x+N_1^x-N_2^x)}{2TN_2^0}s_y^2\\&-\frac{B_3(L^x+N_1^x-N_2^x)}{TN_2^0}\frac{(s_xs_y)^2}{b_1s_x^2+b_2s_y^2}\end{aligned} \tag{E2}$$

with the abbreviations

$$\begin{aligned}&T=1-\tau_1Q\ ,\\&L^x=\epsilon(e_1+2e_2Q)-2r_1Q\ ,\\&L^{xx}=\epsilon(e_2+3e_4Q)-r_1+3r_3Q\ ,\\&L^{yy}=\epsilon(e_3+e_5Q)-r_2+r_4Q\ ,\\&N_2^0=-F^2[1-(a_1-a_2)Q]\ ,\\&N_1^x=F^2[a1+(2a_3+2a_5-a_6)Q]\ ,\end{aligned} \tag{E3}$$

$$\begin{aligned}&N_2^x=F^2[a_2-(2a_4-a_6)Q],\quad N_1^{xx}=F^2a_3\ ,\\&N_1^{yy}=F^2[a_7+(a_{11}+a_{16}-a_{17})Q]\ ,\\&N_2^{xx}=F^2a_4,\quad N_2^{yy}=F^2[a_8-(a_{12}-a_{18})Q]\ ,\\&B_1=(s_1+s_2Q)F^2(q_2-q_3)\ ,\\&B_2=-(s_1+s_2Q)F^2q_4-s_1F^2Q(q_5-q_6)\ ,\\&B_3=(s_1+s_2Q)F^2[q_1-(2q_3-q_2)Q]\ .\end{aligned}$$

From the notation the origin of the coefficients can be read off: the L's come from the linear operator, the N's come from the cubic terms in Eq. (35), and the B's belong to the mean-flow equation (36). The superscripts x,y correspond to the derivatives with respect to x,y. Only terms up to $\mathcal{O}(Q)$ have been kept. The destabilization line at $Q=0$ and its slope with respect to Q is obtained from $\sigma=0$ (E2). The growth rate is maximal for $s_x=0$, corresponding to a pure zigzag destabilization. The destabilization type can be checked with the help of the criteria given in Eqs. (42) and (43). The needed coefficients $\bar{a}$, $\bar{b}$, $\bar{c}$, $\bar{d}$, and v can be expressed in terms of the quantities defined in (E3)

$$\bar{a}=2\frac{B_2}{b_1}-2\frac{B_1}{b_1}+\frac{B_3(L^x+N_1^x-N_2^x)}{b_1N_2^0}\ ,$$

$$\bar{b}=2\frac{B_1}{b_1}-\frac{B_3(L^x+N_1^x-N_2^x)}{b_1N_2^0}\ ,$$

TABLE I. (a) Linear and (b) nonlinear coefficients of Eqs. (35) and (36) for two different electrical anisotropies σ_a (0.7, 0.8) and frequencies $\omega\tau_0$ (0.5, 1.0) (zero magnetic field).

	$H_x=0$			
	$\sigma_a=0.7$		$\sigma_a=0.8$	
	$\omega\tau_0=0.5$	$\omega\tau_0=1.0$	$\omega\tau_0=0.5$	$\omega\tau_0=1.0$
	(a)			
T_0	2.30	1.80	2.45	1.96
τ_1	−2.04	−1.99	−2.05	−2.00
τ_2	−1.17	−1.10	−1.19	−1.12
τ_3	−0.633	−0.497	−0.667	−0.558
e_1	3.67	3.52	3.70	3.57
e_2	4.54	4.13	4.63	4.26
e_3	0.859	0.600	0.918	0.667
e_4	2.19	1.84	2.28	1.95
e_5	1.81	1.24	1.95	1.39
e_6	0.379	0.289	0.405	0.317
e_7	0.703	0.453	0.773	0.527
e_8	0.109	0.012	0.135	0.031
r_1	0.981	0.874	1.01	0.906
r_2	0.052	0.134	0.037	0.120
r_3	−2.40	−2.04	−2.50	−2.15
r_4	−0.364	−0.491	−0.337	−0.474
r_5	−1.82	−1.42	−1.92	−1.54
r_6	−1.26	−1.01	−1.32	−1.08
r_7	−0.110	−0.124	−0.106	−0.128
s_1	3.04	2.63	3.15	2.76
s_2	8.25	6.87	8.60	7.28
s_3	−2.26	−1.75	−2.41	−1.91
s_4	4.70	4.19	4.82	4.36
	(b)			
$\sqrt{A_{\text{scal}}}$	0.0558	0.0519	0.0566	0.0521
a_1	−6.31	−6.22	−6.37	−6.31
a_2	0.414	0.278	0.438	0.290
a_3	−8.03	−7.98	−8.12	−8.15
a_4	0.056	0.111	0.040	0.100
a_5	−9.28	−9.11	−9.39	−9.31
a_6	−0.707	−1.31	−0.582	−1.27
a_7	−1.78	−1.95	−1.79	−1.94
a_8	−0.424	0.004	−0.511	−0.111
a_9	−1.13	−1.83	−1.03	−1.70
a_{10}	−1.02	−0.310	−1.17	−0.522
a_{11}	−3.86	−3.88	−3.92	−3.97
a_{12}	0.425	1.03	0.308	0.884
a_{13}	0.310	−3.34	1.00	−2.71
a_{14}	−5.70	−2.51	−6.40	−3.34
a_{15}	−0.138	2.20	−0.563	1.73
a_{16}	−3.72	−4.10	−3.74	−4.15
a_{17}	0.681	0.680	0.728	0.706
a_{18}	−4.06	−1.17	−4.71	−1.91
a_{19}	−5.67	−2.52	−6.37	−3.32
a_{20}	2.68	2.57	2.76	2.61
q_1	−21.2	−22.3	−19.7	−20.4
q_2	46.7	46.0	44.4	43.1
q_3	15.6	14.8	14.9	14.0
q_4	−3.79	−3.96	−4.14	−4.20
q_5	−11.1	−9.71	−10.8	−9.49
q_6	−15.5	−14.5	−16.2	−15.1

TABLE II. (a) Linear and (b) nonlinear coefficients of Eqs. (35) and (36) for two different electrical anisotropies σ_a (0.7, 0.8) and frequencies $\omega\tau_0$ (0.5, 1.0) (nonzero magnetic field $H_x=1$ in reduced units).

	$H_x=1$			
	$\sigma_a=0.7$		$\sigma_a=0.8$	
	$\omega\tau_0=0.5$	$\omega\tau_0=1.0$	$\omega\tau_0=0.5$	$\omega\tau_0=1.0$
	(a)			
T_0	2.15	1.69	2.28	1.84
τ_1	−2.04	−1.99	−2.05	−2.00
τ_2	−1.21	−1.13	−1.22	−1.14
τ_3	−0.064	−0.492	−0.656	−0.531
e_1	3.62	3.48	3.65	3.53
e_2	4.46	4.06	4.55	4.19
e_3	0.838	0.588	0.896	0.654
e_4	2.15	1.81	2.24	1.92
e_5	1.76	1.20	1.89	1.35
e_6	0.363	0.277	0.387	0.304
e_7	0.694	0.448	0.763	0.519
e_8	0.105	0.012	0.131	0.031
r_1	0.938	0.839	0.962	0.869
r_2	0.051	0.131	0.035	0.117
r_3	−2.29	−1.94	−2.37	−2.05
r_4	−0.345	−0.471	−0.319	−0.453
r_5	−1.74	−1.36	−1.84	−1.48
r_6	−1.18	−0.958	−1.24	−1.03
r_7	−0.104	−0.118	−0.100	−0.122
s_1	2.88	2.51	2.98	2.63
s_2	7.80	6.54	8.11	6.92
s_3	−2.11	−1.65	−2.24	−1.79
s_4	4.47	4.01	4.58	4.16
	(b)			
$\sqrt{A_{\text{scal}}}$	0.0574	0.0532	0.0583	0.0534
a_1	−6.27	−6.19	−6.33	−6.28
a_2	0.422	0.283	0.447	0.296
a_3	−7.96	−7.92	−8.05	−8.08
a_4	0.057	0.113	0.040	0.103
a_5	−9.21	−9.04	−9.32	−9.24
a_6	−0.597	−1.22	−0.462	−1.17
a_7	−1.71	−1.82	−1.73	−1.83
a_8	−0.453	−0.092	−0.528	−0.190
a_9	−1.08	−1.65	−0.994	−1.55
a_{10}	−1.03	−0.461	−1.15	−0.639
a_{11}	−3.68	−3.66	−3.74	−3.76
a_{12}	0.294	0.801	0.194	0.677
a_{13}	−0.451	−3.43	0.111	−2.94
a_{14}	−5.25	−2.67	−5.84	−3.36
a_{15}	0.082	1.97	−0.258	1.60
a_{16}	−3.77	−3.97	−3.81	−4.06
a_{17}	0.715	0.672	0.768	0.705
a_{18}	−4.01	−1.56	−4.58	−2.20
a_{19}	−5.27	−2.69	−5.85	−3.36
a_{20}	2.25	2.15	2.31	2.19
q_1	−22.4	−23.3	−20.9	−21.3
q_2	49.0	47.8	46.7	44.8
q_3	16.2	15.3	15.6	14.4
q_4	−4.05	−4.19	−4.45	−4.46
q_5	−11.5	−9.99	−11.2	−9.77
q_6	−16.3	−15.2	−17.1	−15.8

$$\bar{c}=L^{yy}+N_1^{yy}-N_2^{yy}+\frac{(L^x+N_1^x+N_2^x)(L^x+N_1^x-N_2^x)}{2N_2^0}\ ,$$

$$\bar{d}=L^{xx}+N_1^{xx}-N_2^{xx}-\frac{(L^x+N_1^x+N_2^x)(L^x+N_1^x-N_2^x)}{2N_2^0}\ , \tag{E4}$$

$$v=\frac{b_2-b_1}{b_1}\ .$$

The magnitude of v serves as a measure of the anisotropy of the linear operator in the mean-flow equations. Its value is $v=(\alpha_3+\alpha_6)/\alpha_4\approx -0.42$ in MBBA.

Finally we give the expression for the zigzag destabilization line $\epsilon_{zz}(Q)$, which is obtained from Eq. (E2) for $s_x=0$,

$$\epsilon_{zz}(Q)=\frac{r_2+Q(r_2e_1-r_4)}{h0+Q(h1-h2/b_2)}\ , \tag{E5}$$

where the following abbreviations have been introduced:

$$\begin{aligned} h0&=e_3+a_7-a_8-2s_1q_4/b_2\ ,\\ h1&=2a_7e_1-a_{17}+a_{16}-a_{18}-a_7a_2+a_{11}+a_8a_2\\ &\quad -a_8a_1+a_{12}+e_3e_1+e_5+a_7a_1-2a_8a_1\ ,\\ h_2&=2s_1q_5-2s_1q_6+4s_1q_4e_1\\ &\quad +2s_2q_4+2s_1q_4a_1-2s_1q_4a_2\ . \end{aligned} \tag{E6}$$

The quantity b_2 was defined as $b_2=0.5(\alpha_4+\alpha_3+\alpha_6)$ [see Eq. (35) and Appendix D]. The complicated interplay of the higher-order derivative terms in the coupled amplitude equations (35) and (36) is evident and it seems unjustified to disregard any of them. Note that further coefficients would come in if the upper destabilization line were of the skew-varicose type, a possibility which is included in Eqs. (35) and (36).

[1] P. Manneville, *Dissipative Structures and Weak Turbulence* (Academic, New York, 1990).

[2] M. C. Cross and P. C. Hohenberg, Rev. Mod. Phys. **65**, 851 (1993).

[3] F. H. Busse, in *Hydrodynamic Instabilities and the Transition to Turbulence*, edited by H. L. Swinney and J. P. Gollub (Springer, Berlin, 1986).

[4] F. H. Busse, in *Mantle Convection, Plate Tectonics and Global Dynamics*, edited by W. R. Peltier (Gordon and Breach, New York, 1989).

[5] P. G. de Gennes, *The Physics of Liquid Crystals* (Clarendon, Oxford, 1974).

[6] L. M. Blinov, *Electrooptical and Magnetooptical Properties of Liquid Crystals* (Wiley, New York, 1983).

[7] S. A. Pikin, *Structural Transformations in Liquid Crystals* (Gordon and Breach, New York, 1991).

[8] W. J. A. Goossens, *Advances in Liquid Crystals* (Academic, New York, 1978), Vol. 3.

[9] E. Dubois-Violette, G. Durand, E. Guyon, P. Manneville, and P. Pieranski, in *Solid State Physics, Suppl. 14*, edited by L. Liebert (Academic, New York, 1978).

[10] A. Joets and R. Ribotta, in *Cellular Structure in Instabilities*, edited by J. E. Wesfreid and S. Zaleski (Springer, Berlin, 1984).

[11] E. Bodenschatz, W. Zimmermann, and L. Kramer, J. Phys. (Paris) **49**, 1875 (1988).

[12] S. Kai and W. Zimmermann, Prog. Theor. Phys. Suppl. **99**, 458 (1989).

[13] I. Rehberg, B. L. Winkler, M. de la Torre, S. Rasenat, and W. Schöpf, Adv. Solid State Phys. **29**, 35 (1989).

[14] L. Kramer, E. Bodenschatz, W. Pesch, W. Thom, and W. Zimmermann, Liq. Cryst. **5**, 699 (1989).

[15] W. Zimmermann, Mater. Res. Bull. **16**, 46 (1991).

[16] W. Zimmermann and L. Kramer, Phys. Rev. Lett. **56**, 2655 (1986).

[17] A. Joets and R. Ribotta, J. Phys. (Paris) **47**, 595 (1986).

[18] S. Kai, N. Chizumi, and M. Kohno, Phys. Rev. A **40**, 6554 (1989).

[19] E. Braun, S. Rasenat, and V. Steinberg, Europhys. Lett. **15**, 597 (1991).

[20] S. Rasenat, V. Steinberg, and I. Rehberg, Phys. Rev. A **42**, 5998 (1990).

[21] S. Nasuno and S. Kai, Europhys. Lett. **14**, 779 (1991).

[22] S. Nasuno, O. Sasaki, S. Kai, and W. Zimmermann, Phys. Rev. A **46**, 4954 (1992).

[23] J. Lega, in *Patterns, Defects and Materials Instabilities*, Vol. 183 of *NATO Advanced Study Institute, Series E: Applied Sciences*, edited by D. Walgraef and N. M. Ghoniem (Kluwer Academic, Dordrecht, 1990).

[24] S. Kai and K. Hirakawa, Prog. Theor. Phys. Suppl. **64**, 212 (1978).

[25] A. C. Newell, T. Passot, and M. Souli, J. Fluid Mech. **220**, 187 (1990).

[26] E. Dubois-Violette, P. G. D. Gennes, and O. J. Parodi, J. Phys. (Paris) **32**, 305 (1971).

[27] H. Haken, *Synergetics* (Springer-Verlag, Berlin, 1978).

[28] M. C. Cross, Phys. Fluids **23**, 1727 (1980).

[29] A. C. Newell, T. Passot, and J. Lega, Annu. Rev. Fluid Mech. **25**, 399 (1993).

[30] S. Chandrasekhar, *Liquid Crystals* (Cambridge University Press, Cambridge, 1977).

[31] M. J. Stephen and J. P. Straley, Rev. Mod. Phys. **46**, 617 (1974).

[32] E. F. Carr, Mol. Cryst. Liq. Cryst. **7**, 253 (1969).

[33] W. Helfrich, J. Chem. Phys. **51**, 4092 (1969).

[34] P. A. Penz and G. W. Ford, Phys. Rev. A **6**, 414 (1972).

[35] W. Zimmermann, Ph.D. thesis, Universität Bayreuth, 1988.

[36] E. Bodenschatz, Ph.D. thesis, Universität Bayreuth, 1989.

[37] Q. Feng, W. Pesch, and L. Kramer, Phys. Rev. A **45**, 7242 (1992).

[38] Q. Feng, W. Decker, W. Pesch, and L. Kramer, J. Phys. (Paris) II **2**, 1303 (1992).

[39] S. Rasenati, Ph.D. thesis, Universität Bayreuth, 1991.

[40] W. Eckhaus, *Studies in Nonlinear Stability Theory* (Springer, New York, 1965).

[41] W. Pesch and L. Kramer, Z. Phys. B **63**, 121 (1986).

[42] R. M. Clever and F. H. Busse, J. Fluid Mech. **65**, 625 (1974).

[43] A. Zippelius and E. Siggia, Phys. Fluids **26**, 2905 (1983).

[44] M. C. Cross and A. C. Newell, Physica D **10**, 299 (1984).

[45] A. C. Newell and J. A. Whitehead, J. Fluid Mech. **28**, 279

(1969).
[46] L. A. Segel, J. Fluid Mech. **38**, 203 (1969).
[47] L. Kramer, E. Bodenschatz, W. Pesch, and W. Zimmermann, in *The Physics of Structure Formation,* edited by W. Güttinger and G. Dangelmayr (Springer, Berlin, 1987).
[48] E. Bodenschatz, W. Pesch, and L. Kramer, Physica D **32**, 135 (1988).
[49] L. Kramer, E. Bodenschatz, and W. Pesch, Phys. Rev. Lett. **64**, 2588 (1990).
[50] M. Kaiser, Diploma thesis, Universität Bayreuth, 1988.
[51] E. Bodenschatz, M. Kaiser, L. Kramer, W. Pesch, A. Weber, and W. Zimmermann, in *New Trends in Nonlinear Dynamics and Pattern Forming Phenomena: The Geometry of Nonequilibrium,* Vol. 237 of *NATO Advanced Study Institute, Series B: Physics,* edited by P. Coullet and P. Huerre (Plenum, New York, 1989).
[52] M. Kaiser, W. Pesch, and E. Bodenschatz, Physica D **31**, 212 (1992).
[53] A. J. Bernoff, Eur. J. Appl. Math (to be published).
[54] S. Sasa, Prog. Theor. Phys. **83**, 824 (1990).
[55] S. Sasa, Prog. Theor. Phys. **84**, 1009 (1990).
[56] S. Sasa (unpublished).
[57] M. C. Cross, Phys. Rev. A **27**, 490 (1983).
[58] A. C. Newell, in *Propagation in Systems Far From Equilibrium,* edited by J. E. Wesfried, H. R. Brand, P. Manneville, G. Albinet, and N. Boccara (Springer, Berlin, 1988).
[59] J. L. Ericksen, Arch. Ration. Mech. Anal. **4**, 231 (1960).
[60] F. M. Leslie, Q. J. Mech. Appl. Math. **19**, 357 (1966).
[61] F. C. Frank, Discuss. Faraday Soc. **25**, 19 (1958).
[62] O. Parodi, J. Phys. (Paris) **31**, 581 (1970).
[63] F. H. Busse and E. W. Bolton, J. Fluid Mech. **146**, 115 (1984).
[64] W. Thom, Diploma thesis, Universität Bayreuth, 1988.
[65] W. Decker, Diploma thesis, Universität Bayreuth, 1989.
[66] S. Chandrasekhar, *Hydrodynamic and Hydromagnetic Stability* (Clarendon, Oxford, 1961).
[67] F. H. Busse and R. M. Clever, J. Fluid Mech. **91**, 319 (1979).
[68] Q. Feng, Ph.D. thesis, Universität Bayreuth, 1992.
[69] W. Pesch, W. Decker, Q. Feng, M. Kaiser, L. Kramer, and A. Weber, in *Nematics: Mathematical and Physical Aspects,* Vol. 332 of *NATO Advanced Study Institute, Series C: Mathematical and Physical Sciences,* edited by J. M. Coron, F. Helein, and J. M. Ghidaglia (Kluwer Academic, Dordrecht, 1991).
[70] V. Steinberg (private communication).
[71] M. Kaiser, Ph.D. thesis, Universität Bayreuth, 1992.
[72] J. Carr, *Applications of Center Manifold Theory,* Applied Mathematical Sciences Vol. 35 (Springer, Berlin, 1981).
[73] J. D. Crawford, Rev. Mod. Phys. **63**, 991 (1991).
[74] J. D. Crawford and E. Knobloch, Annu. Rev. Fluid. Mech. **23**, 341 (1991).
[75] P. Manneville and J. M. Piquemal, Phys. Rev. A **28**, 1714 (1983).
[76] L. I. Berge, G. Ahlers, and D. S. Cannell (private communication).
[77] P. C. Hohenberg and B. I. Shraiman, Physica D **27**, 109 (1989).
[78] B. I. Shraiman, A. Pumir, W. van Saarlos, P. C. Hohenberg, H. Chaté, and M. Holen, Physica D **57**, 241 (1992).
[79] A. Tschammer, Diploma thesis, Universität Bayreuth, 1992.
[80] I. Rehberg, S. Rasenat, and V. Steinberg, Phys. Rev. Lett. **62**, 756 (1989).
[81] R. B. Meyer, Phys. Rev. Lett. **22**, 918 (1969).
[82] W. Thom, W. Zimmermann, and L. Kramer, Liq. Cryst. **4**, 309 (1989).
[83] N. V. Madhusudana, V. A. Raghunathan, and K. R. Sumarthy, Pramana J. Phys. **28**, L311 (1987).
[84] A. Joets and R. Ribotta, in *Propagation in Systems Far From Equilibrium,* edited by J. E. Wesfried, H. R. Brand, P. Manneville, G. Albinet, and N. Boccara (Springer, Berlin, 1988).
[85] W. Zimmermann, in *Nematics: Mathematical and Physical Aspects* (Ref. [69]).
[86] W. Decker and W. Pesch, J. Phys. (France) II (to be published).

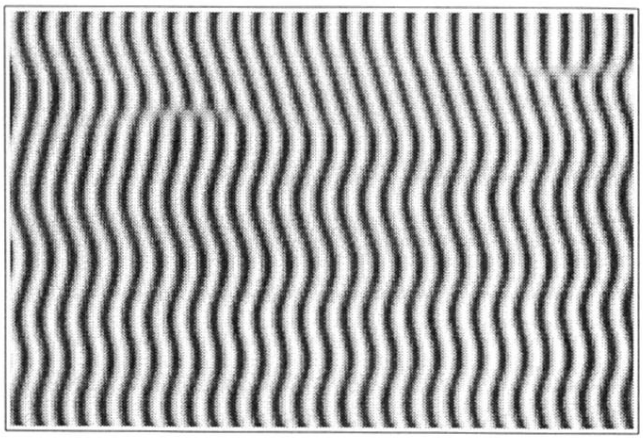

FIG. 10. Snapshot of a 2D simulation pattern (see text) for $\epsilon=0.1$ (the parameters are the same as in Fig. 1) starting from random initial conditions.

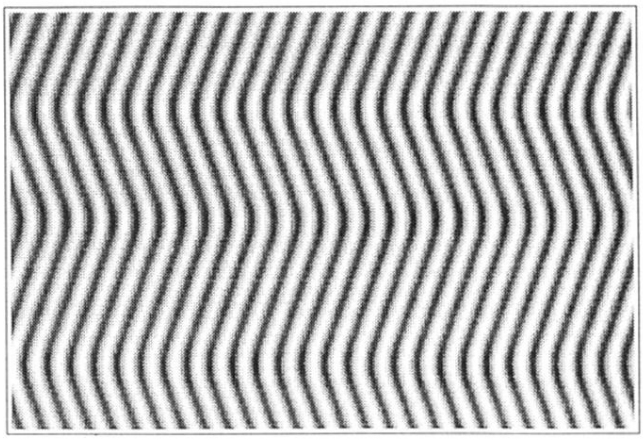

FIG. 11. Snapshot of a stable zigzag pattern (see text) for $\epsilon = 0.1$ (the parameter is the same as in Fig. 1).

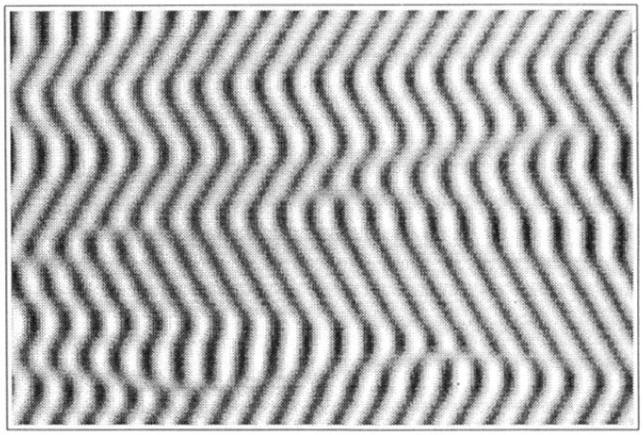

FIG. 12. Snapshot of a 2D simulation pattern for $\epsilon=0.2$ (the parameter is the same as in Fig. 1).